SCIENTIFIC REPORT
on phase 2016 of the project PN-II-ID-PCCE-2011-2-0028
(contract no. 4 / 30.05.2012)

BIOLOGICALLY INSPIRED SYSTEMS FOR ENGINEERED STRUCTURAL AND FUNCTIONAL ENTITIES

Year	Stage	Objectives	Activities	Stage deliverables
2016	unique	**1. The design and development of injectable macromolecular biomimetic matrices for transfection**	1.1. Development and characterization of injectable structured composites, able to load and transport nucleic acids	3 ISI papers 2 participations in scientific conferences 1 patent pending
		2. Assessment of the transfection ability of the systems developed during the project	2.1. Evaluation of complexing capacity of the non-viral vectors versus DNA	
			2.2. Testing of the transfection systems for cell culturing	
		3. The evaluation of transfection ability of the structured composites loaded with polyplexes	3.1. The evaluation of transfection ability of the structured composites loaded with polyplexes	
		4. Development of electrochemical protocols for testing the transfecting systems produced during the project	4.1. The electrochemical evaluation of entities able to sustain transfection	

Objective 1. The design and development of injectable macromolecular biomimetic matrix for transfection

1.1. Development and characterization of injectable structured composites, able to load and transport nucleic acids

This objective was to synthesize and characterize hydrogels based on G4 self-assembly.

A particular attention is being paid to the bioresponsive polymer-based hydrogels, especially in the field of time/spatial controlled release. It is known that hydrogels from polyvinyl alcohol (PVA) have attracted considerable attention because of their high degree of swelling in water, inherent low toxicity, good biocompatibility, and other desirable properties such as transparency and easy handling and PVA-borate-based hydrogels were successfully used as a glucose-sensitive insulin delivery systems for temporary encapsulation of cell.[1,2] The chemistry involved in the crosslinking of PVA using borax consists of di-diol complexation that is originating from one monoborate and two adjacent diol groups of PVA. The formation of these complexes is very fast, which is unusual in the domain of gels and complexing polymers.[3]

In this direction, a supramolecular assembly based approach could be a powerful tool for the producing of ordered microporous hierarchical architectures. Among most known supramolecular assemblies, formation of G-quartets (G4) play by far an important role in aqueous media. Analogues of guanosine (G), have also long been known to form strong hydrogels, typically involving G4·M+ quartet.[4–7] The overall mechanism being represented by initial hydrogen bond-directed assembly of G-quartet units stabilized by K^+, Na^+ or Ba^{2+} ions followed by the formation of ordered ribbon-type or cyclic supramolecular architectures. The combination of the PVA-boric gelation mechanism with the presented assembly techniques could potentially lead to the new hydrogel materials with controlled structure and a vast possibility for the predictable tuning of the gel internal structure by controlling the self-assembly processes. Cyclodextrins, well known for their properties of to form host-guest complexes between the hydrophobic cavity of cyclodextrins and guest molecules have been explored in fields of supramolecular chemistry,[8–10] pharmaceutical[11] and biomedical science[12,13] can bring an interesting feature if incorporated in G4 gels. We established an easy procedure to preparation of hydrogels based on formation of G4 architecture of guanosine grafted on polyvinyl alcohol boric acid (PVAB) through boric ester dynamic link. We showed that introduction of β-cyclodextrin (βCD) to the hydrogels changes its properties, acting as an adjuvant, due to formation of inclusion complexes with guanosine (Figure1). Hydrogels were prepared in straightforward fashion, starting with grafting of guanosine on polyvinyl alcohol boric acid (PVAB) in presence of lithium hydroxide (LiOH) *via* boric acid-diol

complexation resulting in the formation of dynamic covalent crosslinks in compound (Figure 1-2) which is free-flowing solution and by adding potassium chloride the formation of hydrogel occurs.

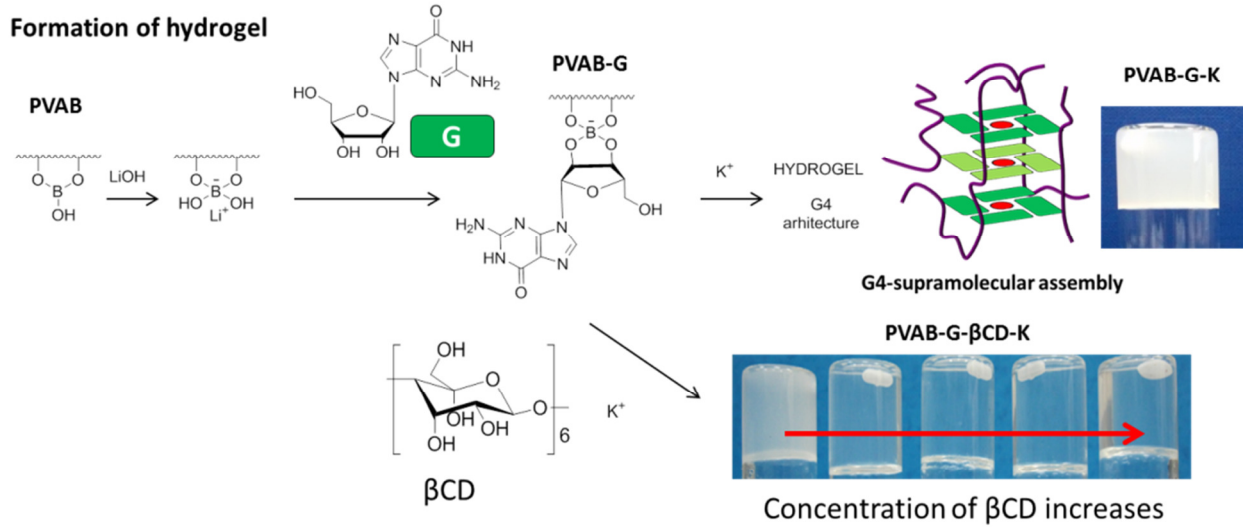

Figure 1. *Schematic representation for the formation of hydrogels.* *^{11}B NMR spectroscopy has been applied to characterize formation of borate esters between PVAB and guanosine. By ^{1}HNMR was proved the formation of inclusion complexes between guanosine and βCD.*

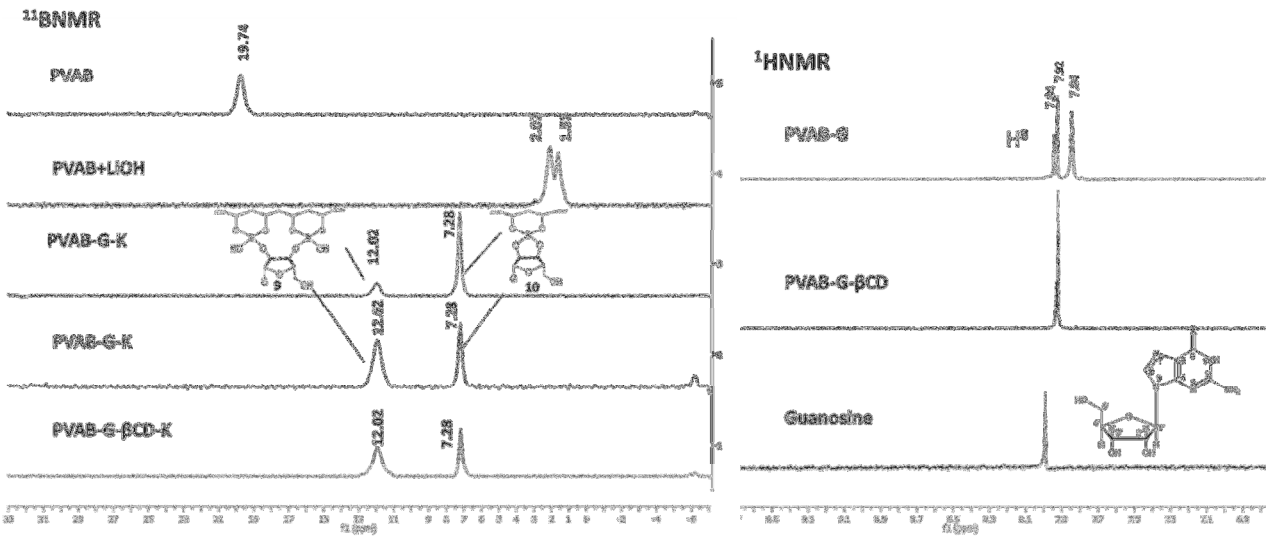

Figure 2. *^{11}B NMR and ^{1}HNMR in D_2O for the obtained compounds.* *PVAB-G forms a supramolecular ordered hierarchical polymer architectures only driven by presence of cation like K^+, Na^+ or Ba^{2+}.*

Circular dichroism (CD) spectroscopy (Figure 3) is often used to identify G-quadruplex structures and in particular to distinguish all-parallel structures from antiparallel structures.[14,15] In general, a peak around 260 nm and a trough around 240 nm imply the presence of a parallel G-quadruplex structure. We observed the G- quartet formation for PVAB-G-K and PVAB-G-βCD-K and not for PVAB-G. Presence of the positive bands in the region of 290 nm could indicate that there is a well-defined stacking of the G-quartets within the hydrogel structure.

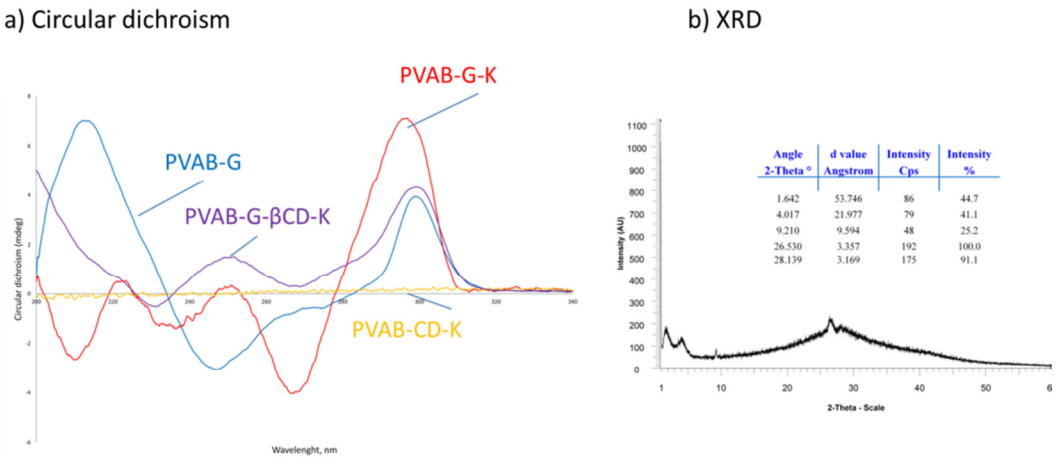

Figure 3. *a) Circular dichroism data. b) X-Ray Diffraction spectrum of PVAB-G-K.*

We have extended characterization of the hydrogel by using X-ray diffraction to obtain molecular-level evidence for G4-quartet formation and stacking of G4-quartet units (Figure 3). XRD data obtained from a freeze-dried sample of hydrogel PVAB-G-K showed a significant peak at 2θ ≈ 26.5° (d = 3.3 Å), which is in line with the π–π stacking distance between two planar G4-quartets. A signal at 2θ ≈ 4.01° with a corresponding distance of 21.97 Å, coordinated with the width of a single G4-quartet.

Presence of guanosine in obtained gels showed a hydrogel characteristic structure while analyzing by SEM (Figure 4). Presence of K^+ changed the morphology of obtained PVAB-G-K and PVAB-G-βCD-K gels to more dense and compact structure.

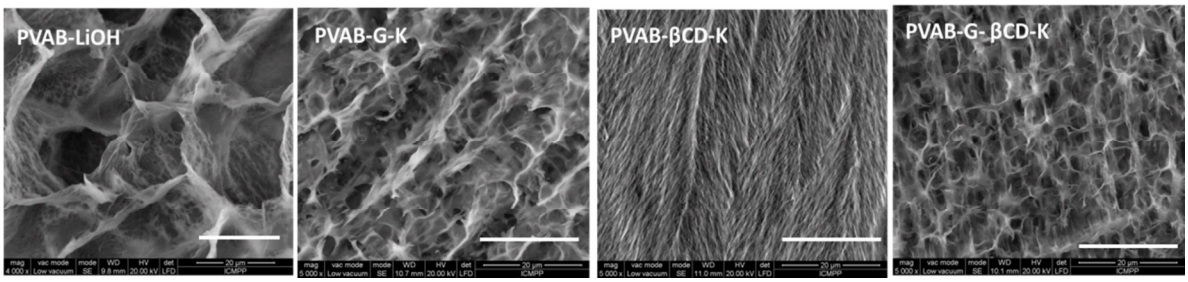

Figure 4. *SEM analysis (scale bar 20 µm).*

Dynamic oscillatory testing is a recognized way to reveal interesting data about microstructure of the materials and to correlate it with the macroscopic behavior (Figure 5). Thus, parameters like complex modulus (G*), storage and loss moduli (G' and G"), loss factor (tan δ=G"/G'), complex viscosity (η*) or phase angle (δ) can be determined obtaining an insight in the internal structure of the sample within the limits of the linear viscoelastic domain.

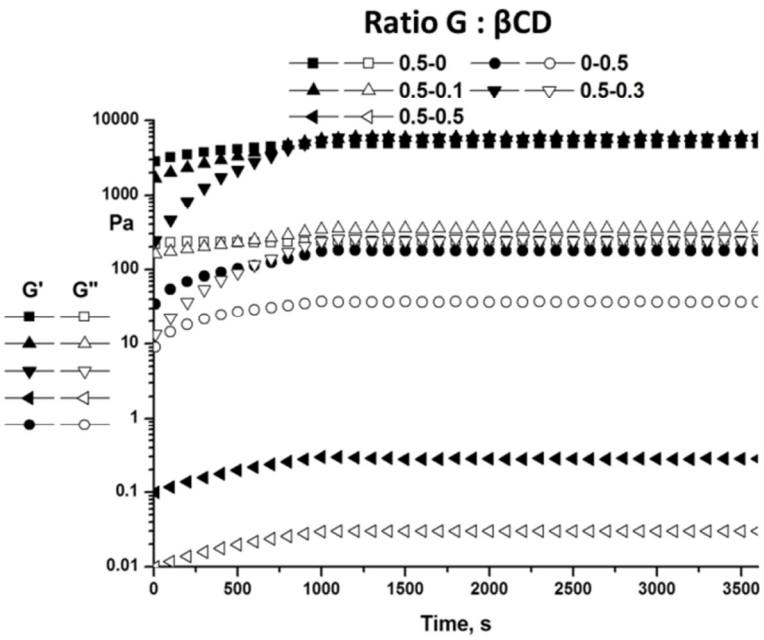

Figure 5. *Time test for the synthesized gels.*

For all samples G' increases fast and reaches a constant plateau after less than 700 s, an indication of the completion of gelation. Moreover it is clear that the ratio of G to β-CD has a clear influence on the rigidity and stability of the resulted hydrogel. The softer gel is obtained for PVAB-G-βCD-K (0.5:0.5) while the hardest and most stable structure is characteristic for PVAB-G-K.

In conclusion was:

- Established an easy protocol for preparation of hydrogels based on G-quartet assembly
- Proved the formation of boronic esters by ^{11}BNMR
- Proved the formation of G-quartet/quadruplex assembly (Fluorescence, CD, XRD)
- Established the mode of interaction of βCD with hydrogel components, i.e. formation of inclusion complex with guanosine
- Studied some hydrogel properties (rheology, SEM)

Objective 2. Assessment of transfection ability of the systems developed by the project

2.1. Evaluation of complexing capacity of the non-viral vectors versus DNA
2.2. Testing of the transfection systems in cell culture

Gene delivery is one of the recent most promising therapeutic methods for the treatment of genetic disorders and acquired diseases (viral infection, autoimmunity - rheumatoid arthritis, cancer, diabetes, coronary, and artery disease) using natural or synthetic nucleic acids to replace / inhibit the faulting gene in cells. The direct transfer of DNA to cells or tissues involves the use of two major types of vectors: viral and non-viral. The choice of a suitable strategy for genetic material delivery to the targeted cells is very important. Non-viral vectors - in the form of organic (proteins, lipids and cationic polymers), inorganic (magnetic nanoparticles, quantum dots, carbon nanotubes, gold nanoparticles, etc.) or hybrid materials - have attracted an increasing interest in last years as an alternative path for transient gene delivery, as they are rather stable and safe, simple to prepare and modify and can be designed/produced in a wide range of sizes and varieties for efficiently passing through biological barriers, as compared to viral vectors.[16,17] However, comparative to viral vectors they suffer from lower transfection efficiency, requiring often additional effort for their optimization. Thus, the design of efficient gene delivery vectors possessing sustained, high transfection efficiencies together with low cytotoxicity is considered a major challenge for delivering a target gene to specific tissues or cells. Among the most studied non-viral systems are those based on polyethylenimine, an off-the-shelf synthetic cationic polymer, which combines strong DNA compaction capacity with an intrinsic endosomolytic activity.[18] However it suffer of increasing cytotoxicity with molecular weight increase, while transfection efficacy is also increasing. Thus an equilibrium must be reached or alternative solutions must be considered.

Some of the strategies to optimize non-viral gene delivery systems involve the use of:

- **nanotechnology** approaches, allowing the development of multifunctional bioactive carriers with small size (enough to improve their stability and to facilitate the internalization into the cells and entering the nucleus, passing through the cytoplasm and escaping the endosome/lysosome process following endocytosis);
- **natural biomaterials**, considering their unique properties such as biodegradability, biocompatibility, and controlled release, emphasizing the lowering of risk of toxicity at high-dose applications;

A. Design, Synthesis and Characterization of Squalene/bPEI gene delivery vector

Typically, strategies to enhance non-viral gene delivery involve complexation of the genetic material with cationic polymers or lipids. Cationic liposomes, cationic lipids, cationic solid lipids, and cationic emulsions are between the most used. The characteristics recommending the lipid inclusion in such carriers refers to:

- self-assembly in an aqueous medium of amphiphiles derivatives/conjugates, i.e. supramolecular organization/self-assembling – properties based on lipid moieties aggregation;
- DNA protection possibility from enzymatic degradation in blood circulation,
- interaction ability with the negatively charged cell membrane to facilitate cell internalization;
- generally slight risk of toxicity at moderate dose applications;
- DNA condensing ability into nanometric colloidal particles able to transfect mammalian cells under *in vitro* conditions;
- low immunogenicity.

However some disadvantages, such as toxicity at high dose, difficult preparation, low transformation efficiency are also to mention.

In an attempt to develop new efficient, safe, biocompatible nanocarriers for therapeutic molecules (including nucleic acids) neutral or anionic nucleolipids were also developed as an alternative to cationic lipids.

Squalene is a natural lipid, a precursor in the biosynthesis of cholesterol (widely distributed in nature). Recently, Couvreur group made use of its advantages in order to develop "squalenoylation nanotechnology",[19] which use squalene as a building block in order to create a bioconjugate (by connecting with biologically active drug molecule such as gemcitabine, anticancer compound paclitaxel and others), which can self-aggregate in water as nano-assemblies, with high drug payloads and absence of burst release. It was proved that the lipid chain self-assembly may be used to obtain multifunctional nano-particles by the co-self-assembly of the different Sq-based functional components.[20] Thus, this innovative concept for improving efficacy and delivery of poorly soluble therapeutic compounds seems a very promising tool by addressing the associated physicochemical and biopharmaceutical challenges.

Other authors,[21] successfully used squalene derivatives (originating from Sq-COOH, Sq-OH) to construct adaptive DyNAvectors (Dynamic Polymers-Dynamers are polymers linked through reversible bonds and able to response to internal or external factors by components' exchange) for DNA binding *via* constitutional self-assembly of functional polyethylenglicol (PEG), Sq derivative and branched cationic polyethylenimine (*b*PEI800) with the multifunctional aldehyde core/centre (1,3,5-benzenetrialdehyde).

Here a squalene/bPEI based amphiphile was developed and characterized envisaging its application in transfection.

To fulfil the requirements associated to the overcoming of the challenging high known number of biological barriers related to a transfection process specific moieties were included in the envisaged conjugate design, in accordance with literature data (Table 1)

Table 1. Design of gene delivery carrier. Included components and their function.

Component	Aim/envisaged effect
Squalene	- moiety which adds extra condensation by forming stable micellar complexes - may facilitate membrane translocation - provide for better expression in cardiovascular cells=lipid modifications to improve transfection or target cardiovascular tissues Bioconjugation with lipids enables to protect sensitive groups from enzymatic degradation and the coupling of hydrophobic moieties may yield amphiphilic conjugates able to cross the plasma membrane by passive diffusion.
bPEI/LPEI (1.8 kDa)	- electrostatic interaction with DNA, pack efficacy for N/P>2 - provide steric protection from nuclease degradation - seems to have an exceptional property in terms of nuclear localization - toxicity increasing with Mw; lower toxicity for LPEI, low Mw - PEI moiety confers buffering (proton sponge) effect/ facilitates endosomal escape.
PEO moiety	Improved systemic circulation / transport protection/ colloidal stability.
-S-S-	- bioreducible/breakdown within the cytoplasm through inherent redox mechanisms - provides for high transfection efficiencies - little to no demonstrable toxicity; - may improve intracellular trafficking: escape endo-lysosomal pathway/strategy to effect intracellular release of DNA/vector-DNA dissociation increasing gene transfer efficiency.
Guanidinyl moiety	Facilitates cell and nucleus membrane penetration=increasing gene transfer efficiency**.**
FITC	Labelling and visualization of cellular uptake process and release kinetics from complex systems.

Mild preparation conditions (room temperature, usual solvents or aqueous reaction medium) were used, according the reaction schemes 1.

The successful development of the final and intermediates Sq-based compounds was confirmed by spectral characterization (^{1}H-NMR, ^{13}C-NMR, FT-IR) as can be seen in Figures 6-10.

The synthesis started from 1,1,2'-tris-nor-squalene aldehyde, obtained according to literature,[22] by interaction with 2,2'-ethylenedioxy bis(ethylamine) to yield the corresponding Schiff base. As a consequence the specific signals for the aldehyde situated at 9.75 ppm in the ^{1}H-NMR spectrum., at 202.7 ppm in ^{13}C-NMR registration, and at 2715 cm^{-1} and 1728 cm^{-1} (vCH and C=O from saturated aldehyde) in FT-IR, disappeared and were replaced by specific signals for iminic group, at 8 ppm, 167 ppm (N=C) and 1573 cm^{-1}, respectively. The epoxy group presence is also easy to observe, the most important signals being situated at 3.4-3.7 ppm, 71 ppm, 1111 cm^{-1}.

Further modification with N,N'-bis (acryloyl)cistamine may be easy evidenced by the specific signals attributable to amide (6.75 ppm, 74 and 164 ppm,) and vinyl groups (5.7-6.35 ppm, 124, 129 ppm, 3066 and 1620 cm^{-1}). Once the bPEI moiety added, the signals/bands assignable to amine, imine groups and methylenic groups connected to them are predominant, some of the other signals being shielded. However the guanidilation and labelling with FITC can be mainly evidenced in ^{1}H-NMR registration, while the retention of the squalene and other moieties may be confirmed from FT-IR data (Figures 9, 10 and Table 2).

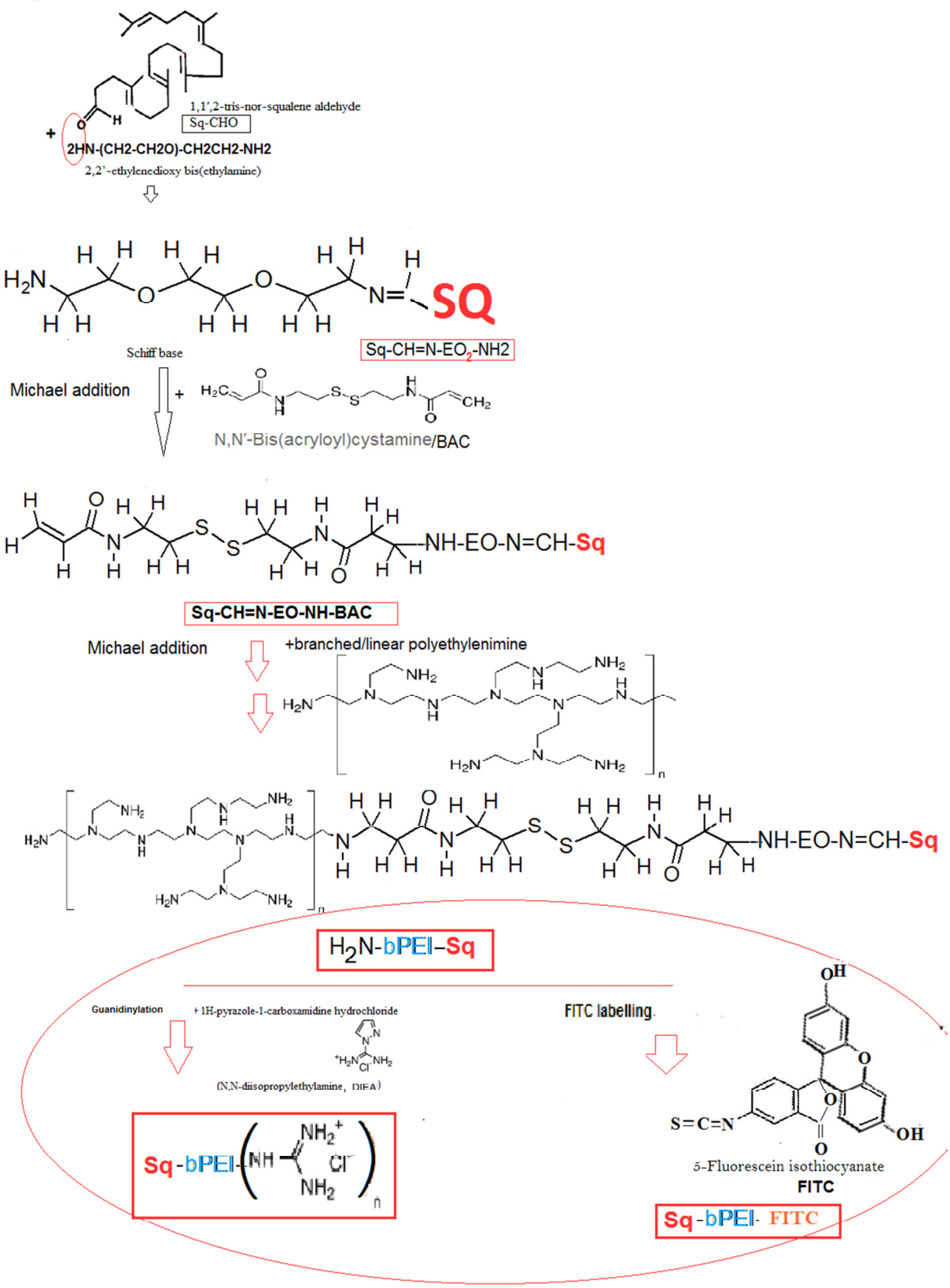

***Scheme 1**. Sq-PEI based carrier synthesis strategy.*

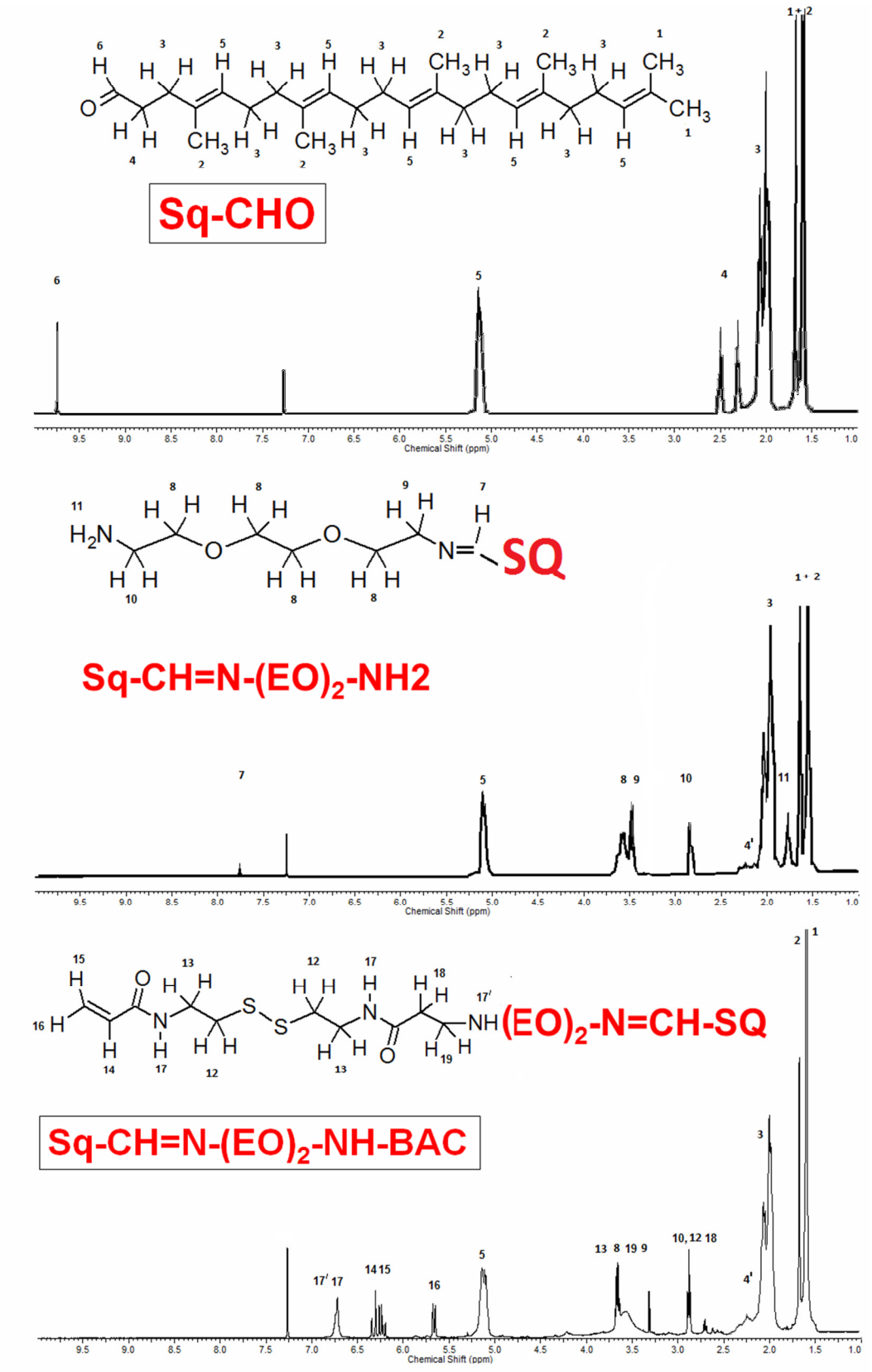

Figure 6. *^{1}H-NMR spectra of the Sq-bPEI intermediates ($CDCl_3$).*

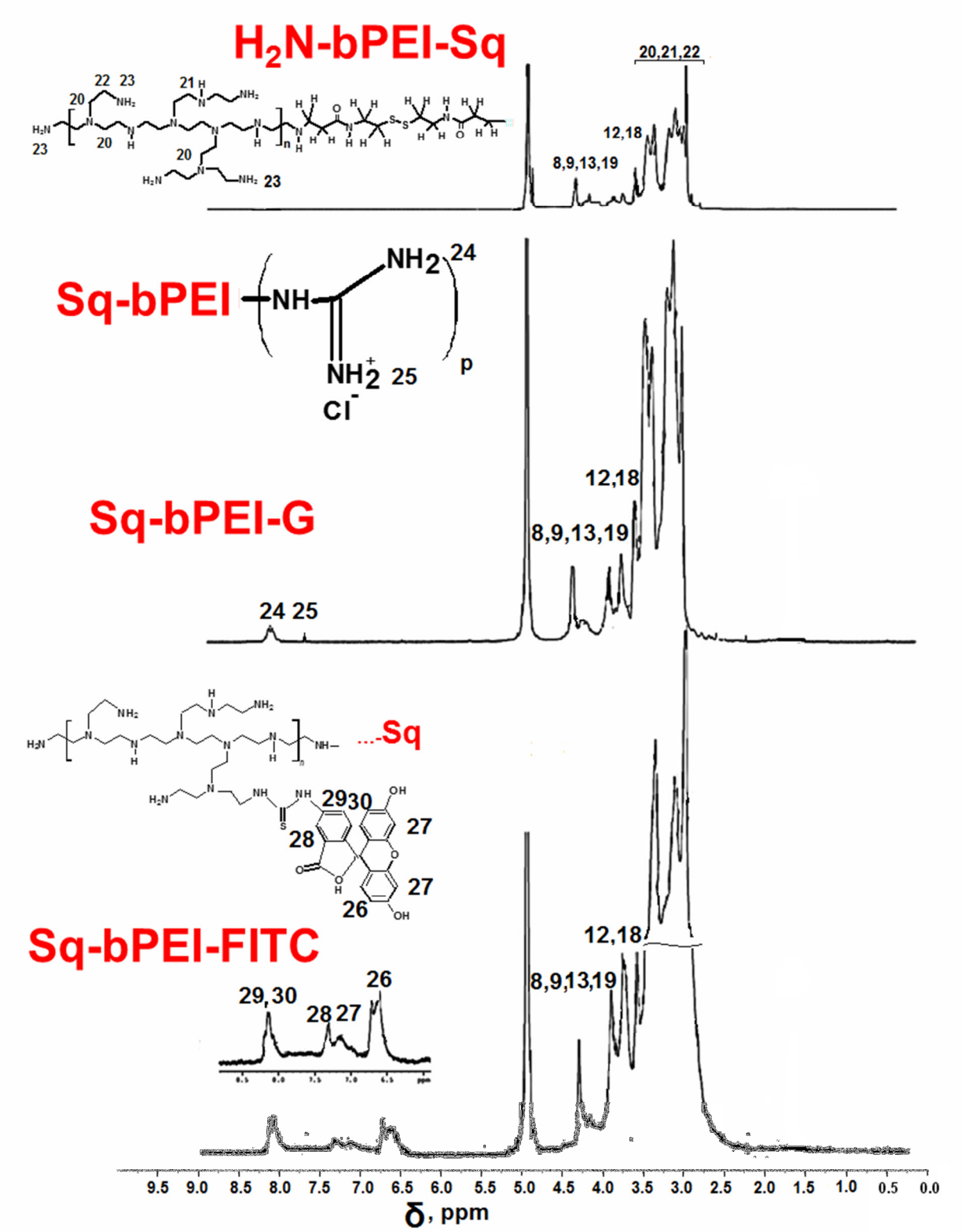

Figure 7. *^{1}H-NMR spectra for the compounds obtained by Sq-bPEI functionalization (D_2O).*

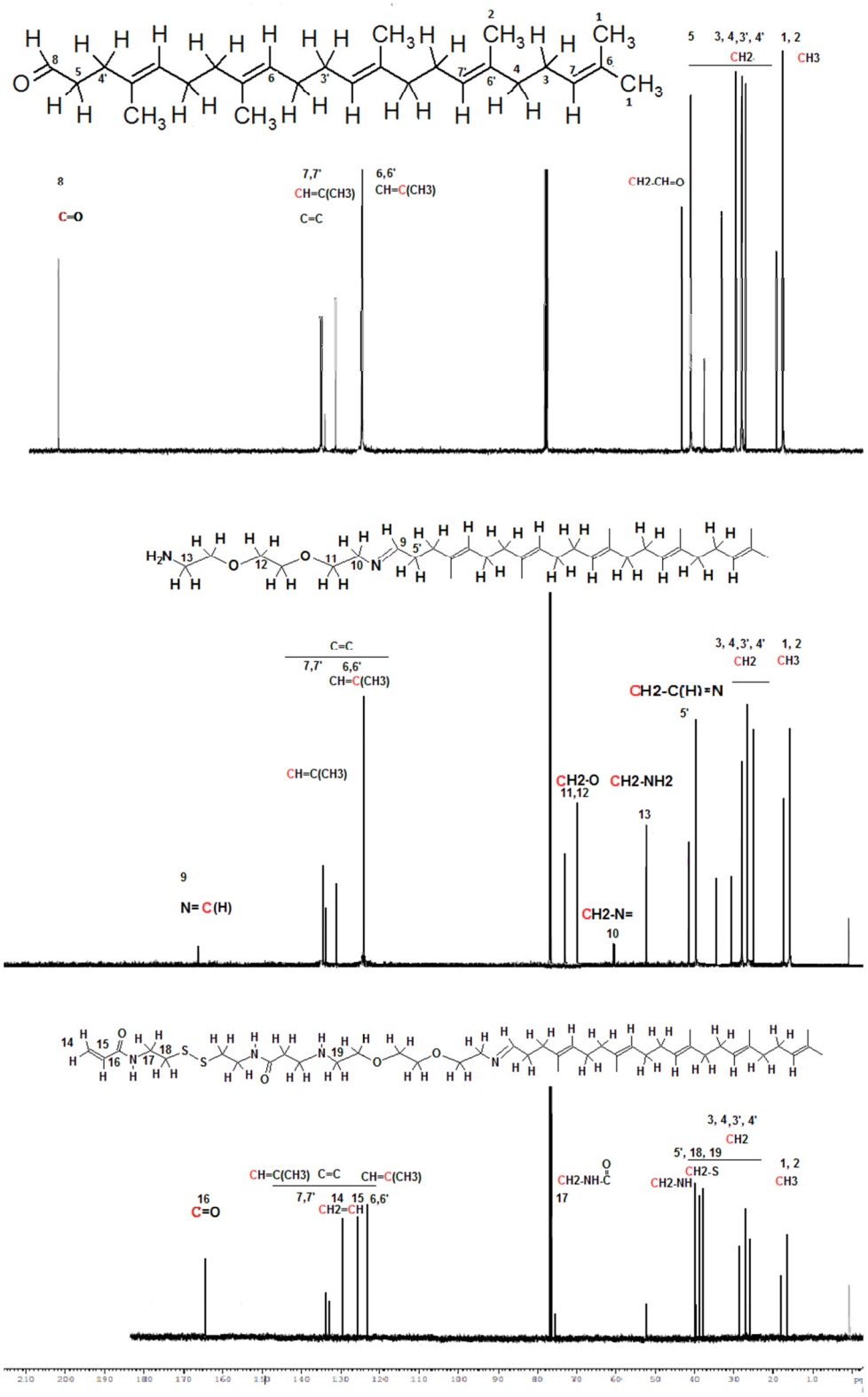

Figure 8. *^{13}C-NMR spectra for the Sq-bPEI carrier and intermediates ($CDCl_3$).*

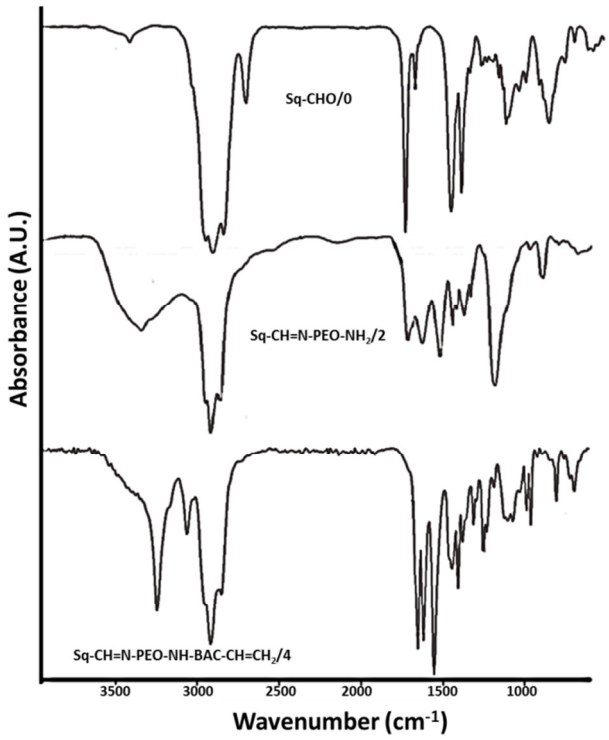

Figure 9. *Typical FT-IR spectra for Sq-PEI and its intermediates.*

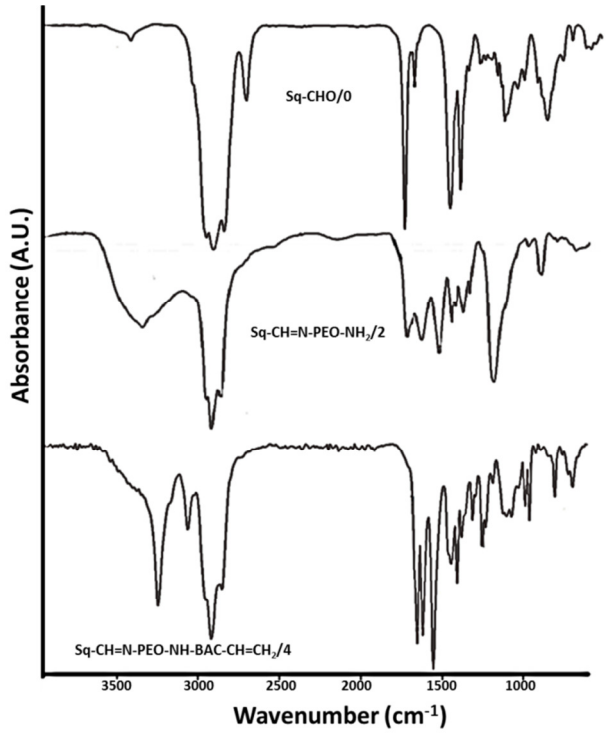

Figure 10. *FT-IR spectra of Sq-PEI and its guanidinilated and FITC labeled derivatives.*

Table 2. Detailed FT-IR data interpretation

Product	Absorption band	Origin of absorption
Sq-CHO/0	2964, 2920, 2854	- v(C-H) asim si sim in (=CH, CH_3, CH_2)
	2715 +2854 (partially)	- v(C-H) aldehyde (saturated)
	1728	- v(C=O) aldehyde (saturated)
	1667	- v(C=C)
	1446, 1382	- δ(C-H)
	1106, 990	- C-H disubstituted alkene (trans)
	898, 838	- C-H trisubstituted alkene
Sq-PEO-NH_2/2	3200-3600/peak la 3363	- v(N-H) in primary amine (NH_2) and (imine NH) (free or implied in H bonds)
	2957, 2925, 2869	- v(=CH, CH_2,CH_3)
	1667.5	- v(C=C) aliphatic
	1573	- v(C=N) imine/Schiff base
	1471,1378	- δ(C-H)
	1309	- v(C-N)
	1111	- C-H disubstituted alkene (trans) + v(C-O-C)
	811	- γ(CH)
Sq-BAC-$CH=CH_2$/4	3200 - 3600 cu peak 3250	- v(N-H) imine/Schiff base (soft) and amide (secondary amide, NH associated by H bonds - 3250)
	3066	- v(C-H) in (=CH_2 vinyl)
	2958, 2923, 2855	- v(=CH, CH_3, CH_2)
	1652	- vC=O amide I (saturated) + v(C=C) aliphatic
	1620	- v(C=C) vinyl
	1553 (mai larg)	- v(C=N) imine+ v(C-N) + NH def (amide II)
	1445,1386	- δ(C-H) (1445 and CH_2-S def)
	1311	- CH_2-S- wag
	1252	- (C-N amide) amide III
	1124	- v anti-sim (C-O)
	1103	- v(C-O) + C-H disubstituted alkene (trans)
	1071	- v(C-S)
	989	- C-H disubstituted alkene (trans)
	962	- δ(H-C-S) bend
	811	- γ(CH)
	696	- v(C-S)

Sq-bPEI/5a	3600-3200 cu peak la 3433.5 2958, 2920, 2852 2480 1647 (wide) 1463 1125 1082-1021 954 850-600	- v(N-H) (NH_2, NH amide and imine free or associated by H binding) - v(C-H) in (=CH, CH_3, CH_2) - protonated form 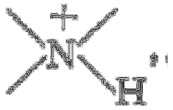 - v(C=O) amide I (saturated) + v(C=C) aliphatic + (NH bend) - (CH) bending - v(C-O-C)+ C-H disubstituted alkene (trans); v(C-N-C) in secondary amine/imine - v(C-S) + v(C-N) in tertiary amine - v(C-N) -NH bend, wide, multiple
Sq-PEI-G/5b	3600-3200 cu peak la 3367 2951, 2840 1651 1618 1459 1082 si 1211 954	- v(N-H) (NH_2, NH in amide and imine) - v(C-H) din (=CH, CH_3, CH_2) - v(C=O) amide I (saturata) + v (C=C) alifatic + NH bend (sh) 1618/1651 coupled δNH/CN in plane for guanidyl group (respective $v_{as}(CN_3H_5^+)$ $v_s(CN_3H_5^+)$) + v(C=N) iminic (Baza Schiff) - forma NH_3^+ in complex - (CH) bending - v(CN), δ(NH) + v (C-O-C) + C-H alkene disubstituted (trans); v(C-N-C) in amine (secondary and tertiary), v(C-S) - v(C-N)
Sq-PEI-FITC /5c	3700-3200 cu peak la 3433 3050 (sh), 2959, 2928, 2850 1650 1636 1573	- v(N-H) (NH_2, NH in amide and imine) - v(C-H) din (=CH vinylidene and aromatic, CH_3, CH_2) - v(C=O) amide I (saturated) + v(C=C) aliphatic + NH bend - v(C=C) aromatic - superposing v(C=C) aromatic and v(C=O) in FITC + [v(C=N) imine + v(C-N) + NH def (amide II)] + amide III in

		secondary thioamide
	1463+1390	- v(C=C) aromatic + v(C=O) sym + δ(C-H)
	1329, 1299 ,1211, 1108	- v(C-O)
	1171	- (C-O) phenol (bend)
	1021	- v(C-S) + v(C-N) in tertiary amine
	954	- (C-H) disubstituted alkene, v(C-N)
	915, 852, 812, 771	- CH aromatic (out of plane) bend
	771	- + NCS def

The DNA binding ability of the Sq-bPEI based compounds was comparatively evaluated against bPEI by agarose gel electrophoresis investigations. Salmon DNA was used.

As can be seen in Figure 11, the DNA compaction ability is decreasing in the order: Sq-PEI-G> Sq-bPEI> bPEI (5b>5a>bPEI (1.8kDa). Optimum N/P ratios found are of about 2, 6 and 7 respectively.

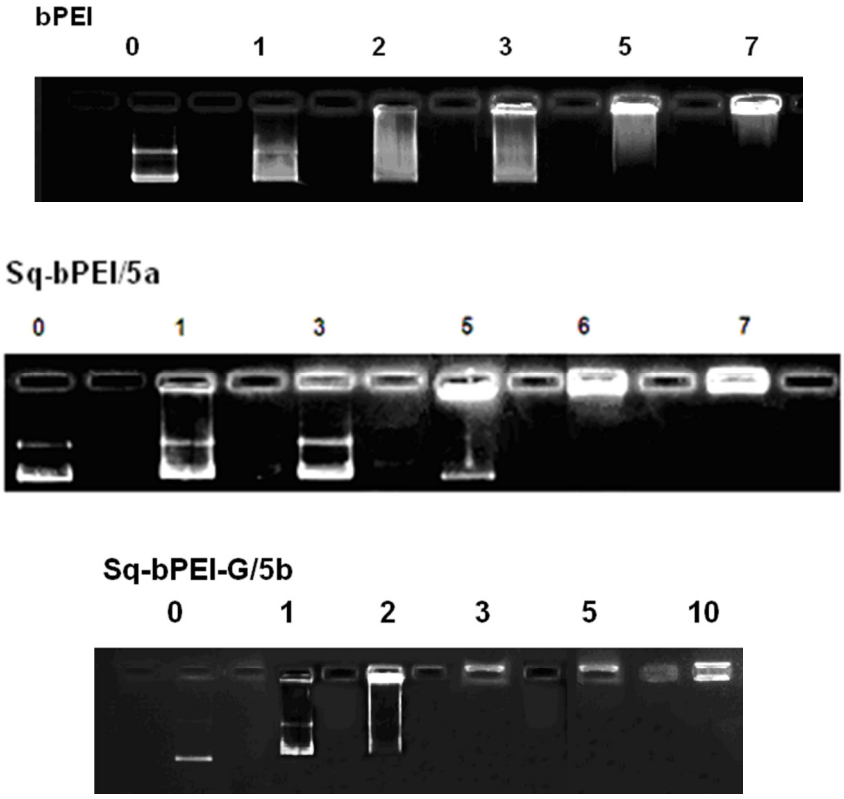

Figure 11. *Agarose gel electrophoresis registrations for the Sq-PEI developed carriers comparative to the used naked bPEI.*

The N/P, respectively polymer carrier/DNA weight ratio is a critical design parameter to control both transfection efficiency and cytotoxicity. The transfection efficiency generally increases as the N/P ratio increases, but the cytotoxicity may also increase. Higher N/P ratios were found to be required in transfection, the free carriers affecting the cellular uptake pathway as well as the intracellular trafficking.[23] Indeed the investigations of transfection of HeLa cells with reporter gene eGFP in the presence of bPEI (1.8 kDa) and the here developed carriers (Sq-bPEI/5a and Sq-bPEI-G/5b) indicated for Sq-bPEI and Sq-bPEI-G optimum values for N/P of 15 for 5b and 20 for 5a (Figures 12, 13). For N/P of 15 Sq-bPEI has a transfection efficiency 6.2 times higher, and Sq-bPEI-G 8.33 times higher than bPEI. For N/P of 20 the Sq-bPEI efficiency increases, becoming 10 times higher than that of bPEI , while the transfection efficiency of Sq-bPEI-G decreases, but still is 5 times higher than that of bPEI. From these data it is obvious that the lipidic moiety aggregation gives rise to increased local accumulation of bPEI chains yielding transfection efficiency increase. As expected from the vector design step guanidilation favored the complexation with DNA and also the penetration of the polyplex through the cell/nucleus membrane.

The cytotoxicity dependence on N/P ratio for the 3 vectors is shown in Figure 14. As can be observed from the presented data the cytocompatibility is enough good and similar for the investigated vectors until a N/P ratio in the range of 10 to 15. Then it is slightly decreasing especially for the Sq-PEI based compounds.

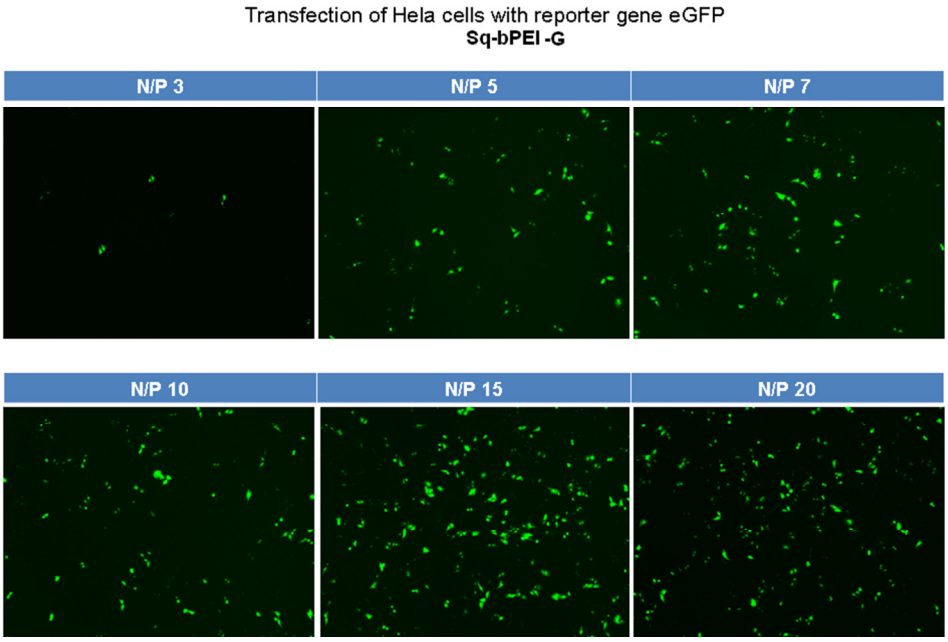

Figure 12. *Fluorescence microscopy micrographs at different N/P values for Sq-bPEI-G and Sq-bPEI during transfection investigations on HeLa cells, with reporter gene eGFP (t=48h).*

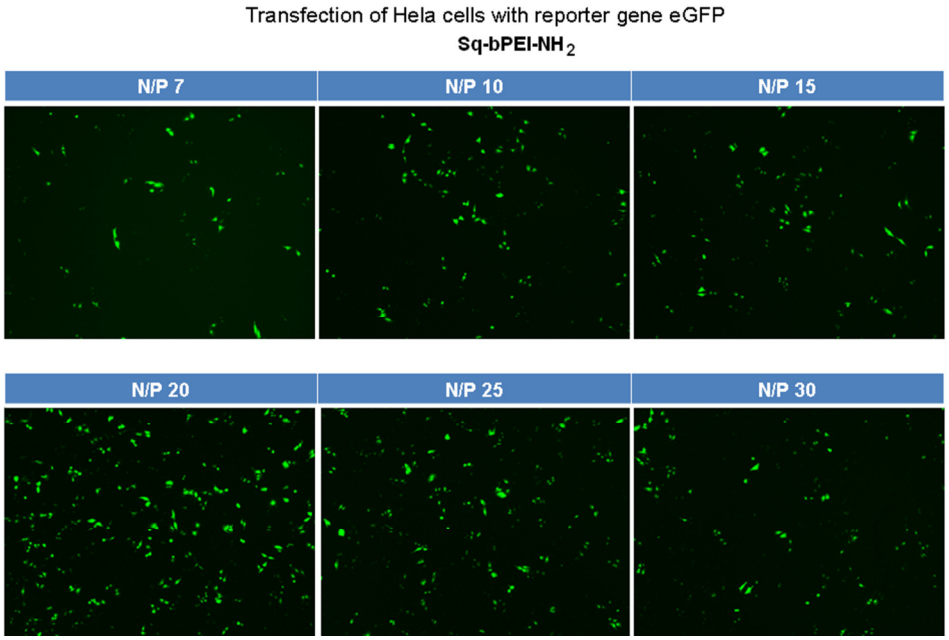

Figure 13. *Comparative representation of Luciferase gene expression for bPEI (1.8 kDa), Sq-bPEI and Sq-bPEI-G.*

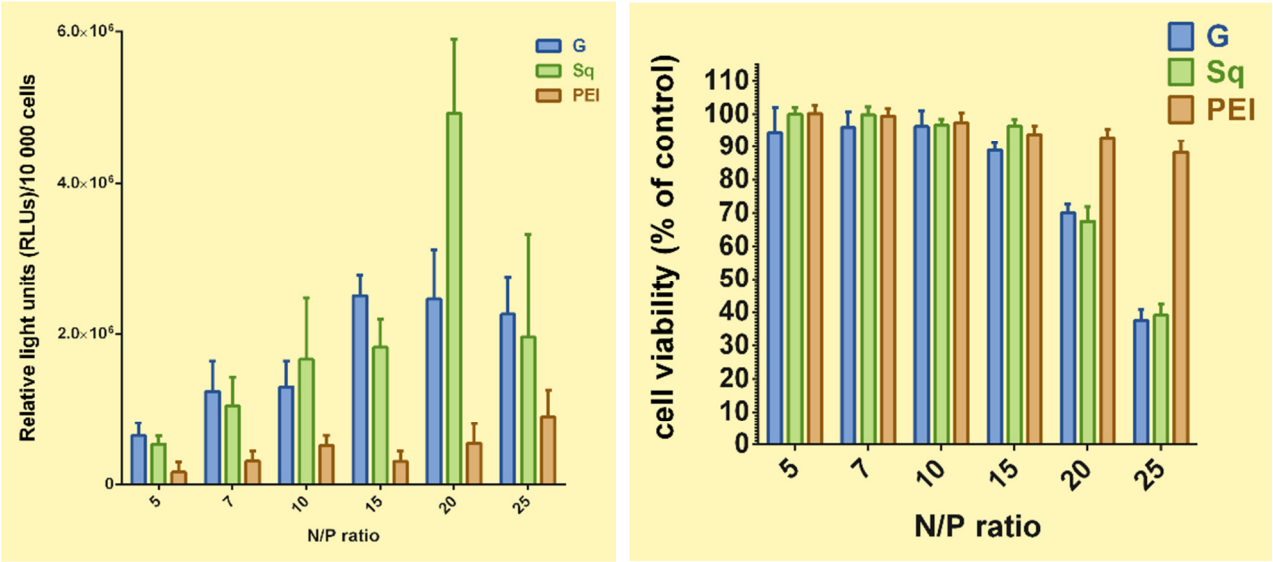

Figure 14. *Comparative cytotoxicity profiles of polyplexes formed with bPEI, Sq-bPEI and Sq-bPEI-G, respectively, based on PI assay.*

B. Non-viral vectors based on imines with hydrophobic/hydrophylic structure by Constitutional Dynamic Chemistry

A literature survey reveals that highly efficient transfection was reached for non-viral vectors with a spherical morphology and high charge density on the surface, the dendrimers being the most appropriates. Moreover, studies dedicated to the structure/

transfection efficiency relationship indicated that very good results were obtained in the case of dendrimers with a high number of generations which contain hydrophobic units within, which facilitated the penetration of the nucleus membrane. On the other hand, the dendrimer synthesis and purification is a quite difficult step, time and effort consuming.

In this context, our objective was to study the possibility of obtaining systems based on hydrophobic/hydrophilic structural blocks connected by imine linkages – reversible bonds which allow reorganizations by imination and trans-imination reactions, under the pressure of the obtaining a stable design with minimum surface energy which are spherical structures (Scheme 2).[24,25]

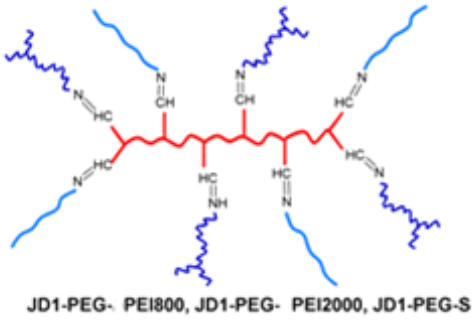

A) **B)**

Scheme 2. A) *Synthesis of non-viral vectors based on polysiloxanic core;* ***B)*** *Graphical representation of the non-viral vectors based on a polyoxipropylenic core*

The success of the synthetic pathway was demonstrated by transmission electronic microscopy (TEM) images, which revealed spherical structures with nanometric diameter which correlate well with the compound structure (Figure 15).

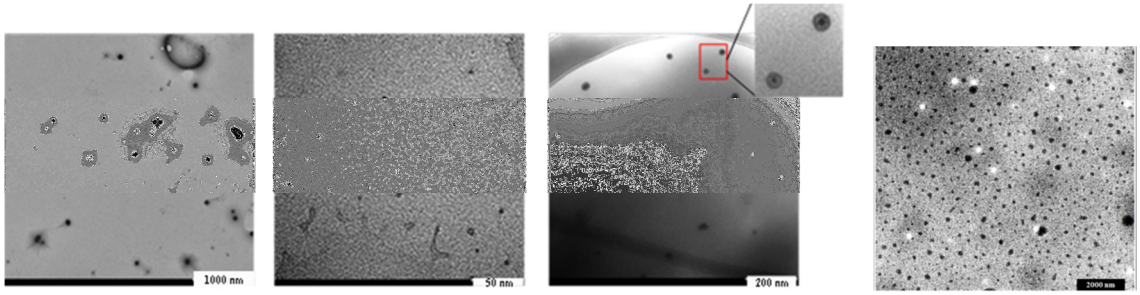

Figure 15. *TEM images of* ***JD1-PEG-PEI800****,* ***JD1-PEI800, JD1-PEI2000, TAS-PEI 2000*** *(from left to right).*

Thus, the compounds based on the polyoxipropylene core and PEI800 (***JD1-PEI 800***) had a diameter of 6 nm, that based on PEI 2000 (***JD1-PEI 2000***) of 23 nm, while

that based on PEG and PEI (***JD1-PEG-PEI800***) of 50 nm. On the other hand, the compounds based on polysiloxanic core and PEI 800 (**TAS-PEI800**) showed an average dimension of 20 nm, and that based on PEI 2000 (**TAS-PEI2000**) of 95 nm (Figure 15).

The synthesized compounds formed polyplexis with DNA from salmon (250 per of basis) and also with DNA double stranded similar to the plasmidic DNA used in gene therapy (4800 per of basis). Their ability to complex the DNA has been followed by electrophoresis on agarose gel permeation. It was established that the compounds based on branched PEI have a better capability to diminish the electrophoretic mobility of the DNA on the agarose gel, starting for small N/P ratios: N/P=1 for ***JD1-PEI 2000***; N/P=3 for ***JD1-PEI 800***; N/P=300 for **TAS-PEI800 and** N/P-30 for (**TAS-PEI2000**). A representative electrophoretic image is given in Figure 16.

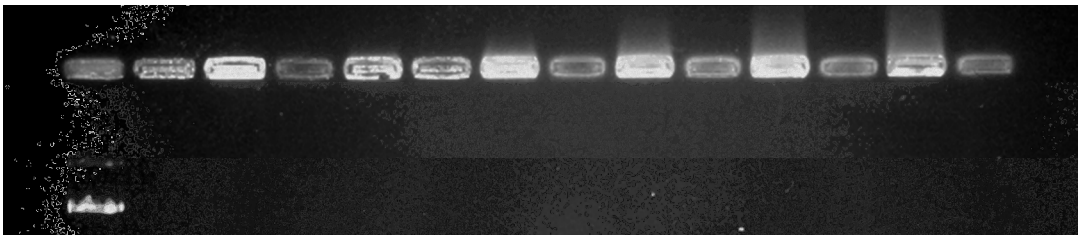

Figure 16. *Electrophoresis on agar gel of* ***JD1-PEI2000****, for the N/P ratios of 1;5;10;50;100;200*

As a general remark, the compounds based on hydrophilic branched PEI demonstrated an excellent transfection efficiency on HEK 293T or HeLa cells, with close values to the SUPERFECT etalon and better values compared to the free PEI (Figure 17). Among them, those based on polysiloxanic core exhibited better transfection efficiency compared to those based on polyoxipropylenic core.

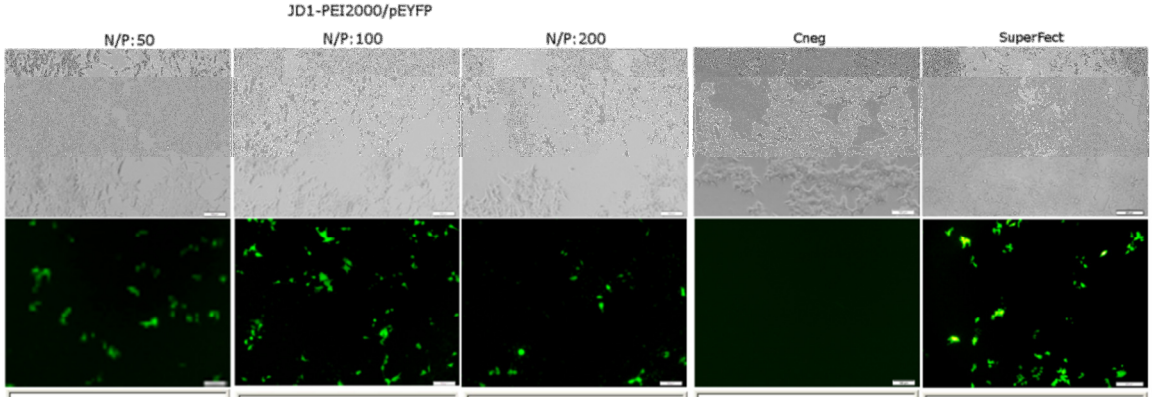

Figure 17. *Visualization of YFP protein expression in HEK 293T cells transfected with* ***JD1-bPEI2000****/pEYFP (left) and* ***bPEI2000****/pEYFP (right) polyplexes at different N/P ratios. Bright fields (upper rows) and the same field of fluorescence images (middle rows) are presented for each polyplex at different N/P ratio. Scale bar 100 µm.*

C. Non-viral vectors based on polyrotaxane structures, as gene delivery systems

The present work have aimed to achieve a gene vehicle with a complex architecture, capable to accomplish a number of requirements, such as the following: to prove a convenient DNA packaging, transport and release, to exhibit a good biocompatibility and clearance, low cytotoxicity and a high transfection efficiency.

All these aims have been satisfied through synergistic interaction of α,ω-bis-propargyl-poly(ethylene oxide) of 1100 Da (PEG_{1100}) with acrylated β-cyclodextrin (acryloyl-β-CD) with acryl unit/CD molar ratio of 3/1 and the propargyl groups of PEG were reacted with 1-(3-brompropyl)silatrane, forming polyrotaxane structures. Later acryloyl groups of β-CD were reacted with primary amine groups of branched polyethylenimine of 2 KDa (PEI_{2000}), via Michael addition, giving a polycationic conjugate with the main role to condense nucleic acids (Figure 18). The branched PEI molecules, mainly those having molecular weights exceeding 25 kDa, have proved an excellent transfection yield, but with the drawback of a poor cytocompatibility. By contrast, PEI of low molecular weight (e.g. PEI_{2000}) has shown proper cell viability, while causing a significant reduction in the rate of transfection.[21,26,27] In this manner a substantial number of PEI_{2000} chains have been brought together to take part in the formation of a single macromolecular entity when a cumulative polycationic segment reached a molecular weight in the range of optimum effectiveness regarding gene transfer, higher than 25 kDa. Moreover by using as end-capped the silatrane azide, as a bulky groups to prevent the slipping out of the β-CD molecules from PEG chain, helps to obtain more antitumoral and antimicrobial effects.[28] The polyrotaxane structure consisted in a non-viral vector with a length of 30 nm and a cross section of around 10 nm, being much closed with histone dimensions; these aspects were demonstrated by molecular dynamics (MD) simulations (Figure 19).

Acrylated β-CD was obtained by the esterification of C-6 hydroxyl groups of glucose units[29] with acryloyl chloride (Figure 18). By adjusting the molar ratio of the two reaction partners, different substitution degree of β-CD can be obtained. The purpose of the esterification (acrylation) reaction is to introduce as reactive acryloyl groups as necessary to attain the most favorable N/P ratios of the final polyplexes that assure the highest transfection capacity. The acrylation of β-CD with 3.5 acrylated groups was confirmed by FTIR, ^{1}H-NMR, ^{13}C-NMR and ^{1}H,^{13}C-HSQC spectroscopy.[30]

The synthesis of polycationic carrier was build based on the Michael addition reaction[29] between the nucleophilic amino groups of branched PEI, and the double-bond of β-CD-acryl from polyrotaxane structures in absolute methanol, after 5 days the methanol was removed at room temperature, after that the product (viscous liquid) was redissolved in bidistilled water and dialyzed with a 3500 MWCO cutoff dialysis membrane for 7 days against double distilled water, followed by lyophilization. The postulated structure of the resulting polycationic carriers is depicted in Figure 18. To prove it, FTIR, NMR, and GPS analyses were performed.

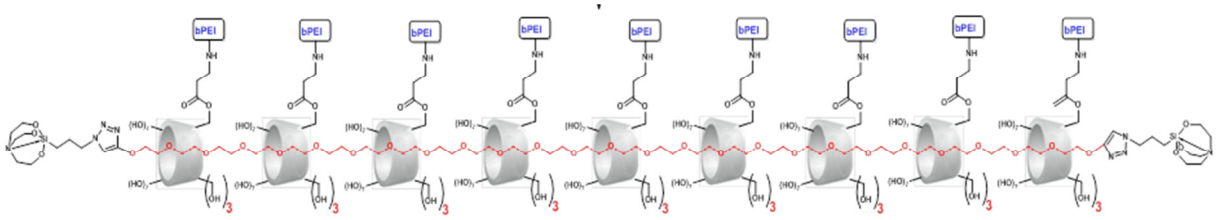

Figure 18. *The synthesis of polyrotaxane structures.*

By comparing the results obtained by NMR and GPS curve of cationic polyrotaxane resulted that the polyrotaxane is composed of PEG_{1000}, β-CD and PEI_{2000} in a molar ratio 1:9:27.

Molecular dynamics (MD) simulations were performed using Maestro simulation environment in a parallelepiped box with 49582 water molecules, 786 Cl^- ions and 138 Na^+ ions, to achieve system neutrality and a 150 mM salt concentration. The equilibrated structure has a rod-like shape with the longitudinal dimension of around ~13.5 nm and a transversal diameter of approximately ~ 6.7 nm, comparable to the in size of histone core of nucleosome dimensions (~6.5 nm). The bi-dimensional charts of the density of different components of the system gives us information about the internal structure of the aggregate. It can be observed the absorption of the negative Cl^- ions and the exclusion of the positive Na^+ ions from the interior of the aggregate.

Results of Molecular Dynamics shown dsDNA: PEI interactions and the minor and the major groves of DNA are not changed by its interaction with PEI macromolecules (Figure 20). This results was confirmed by circular dichroism analyses.

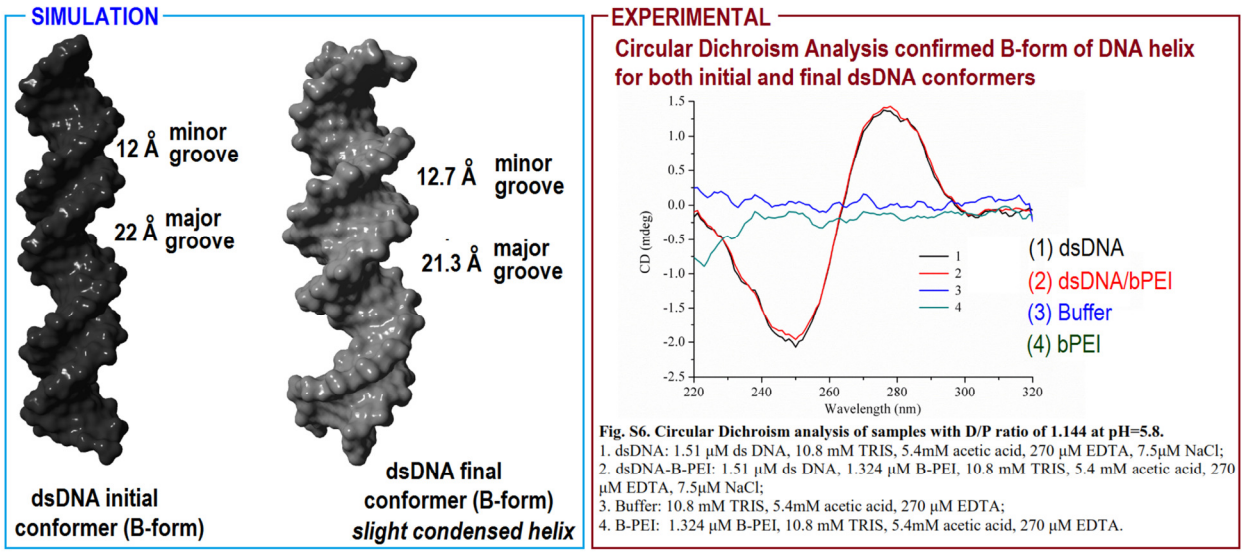

Fig. S6. Circular Dichroism analysis of samples with D/P ratio of 1.144 at pH=5.8.
1. dsDNA: 1.51 μM ds DNA, 10.8 mM TRIS, 5.4mM acetic acid, 270 μM EDTA, 7.5μM NaCl;
2. dsDNA-B-PEI: 1.51 μM ds DNA, 1.324 μM B-PEI, 10.8 mM TRIS, 5.4 mM acetic acid, 270 μM EDTA, 7.5μM NaCl;
3. Buffer: 10.8 mM TRIS, 5.4mM acetic acid, 270 μM EDTA;
4. B-PEI: 1.324 μM B-PEI, 10.8 mM TRIS, 5.4mM acetic acid, 270 μM EDTA.

Figure 20. *Molecular Dynamic Simulation of dsDNA and experimental results by Circular Dichroism before and after interaction of dsDNA with PEI*

Figure 21 shows a comparison between the aggregate and the nucleosome/histone core structures. For the histone core the negatively charged arginine, lysine and histidine residues are represented as van der Waals spheres.

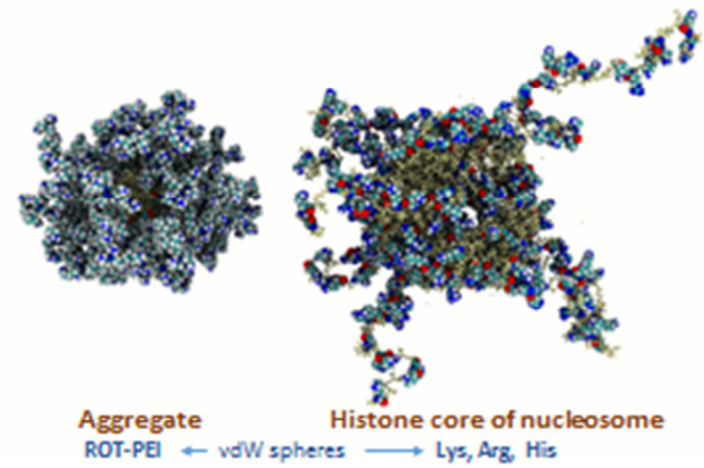

Figure 21. *Representation of polyrotaxane/dsDNA aggregate and histone core of nucleosome.*

MTT assays is an indirect measure of cell viability; measuring the changes in the mitochondrial dehydrogenase integrity, giving a dark blue product. The cytotoxicity of synthesized conjugates and of their polyplexes carrying plasmidic DNA was investigated on HEK 293T cell cultures, using the MTT assay. A cellular viability higher than 95 % was obtained for both uncomplexed polyrotaxane-PEI and its polyplexes with pCS2+MT-Luc (Figure 22).

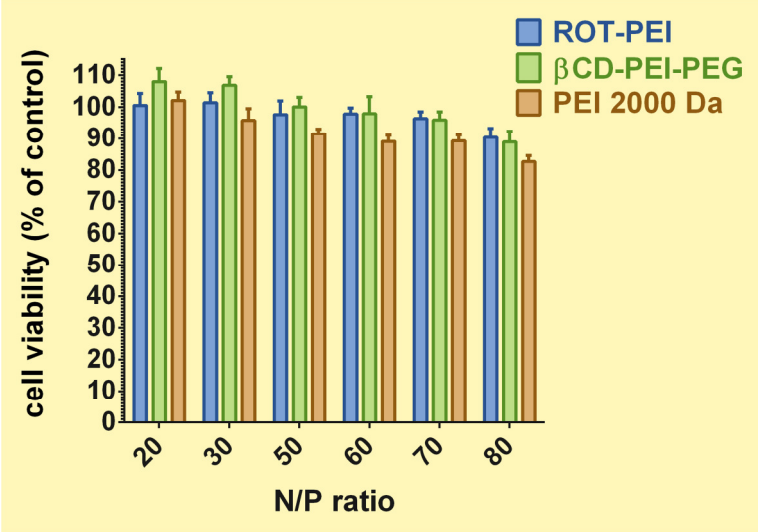

Figure 22. *Cytocompatibility of the carriers.*

The transfection efficiency of the polyplexes based on the synthesized conjugates was determined by two complementary techniques: the fluorescence microscopy, to qualitatively evaluate the abundance of transfected cells (Figure 23), and by the quantification of transfection ability of polyplexes (Figure 24). The used polyplexes are carrying Luciferase gene (pCS2+MT-Luc) able to encode green fluorescent protein (eGFP). HeLa cells were transfected with polyplexes made by combining pCS2+MT-Luc plasmid with polymeric carriers. As it can be observed from Figures 23 and 24 for all tested N/P ratios, ROT-PEI polyplexes manifested the highest transfection efficiency.

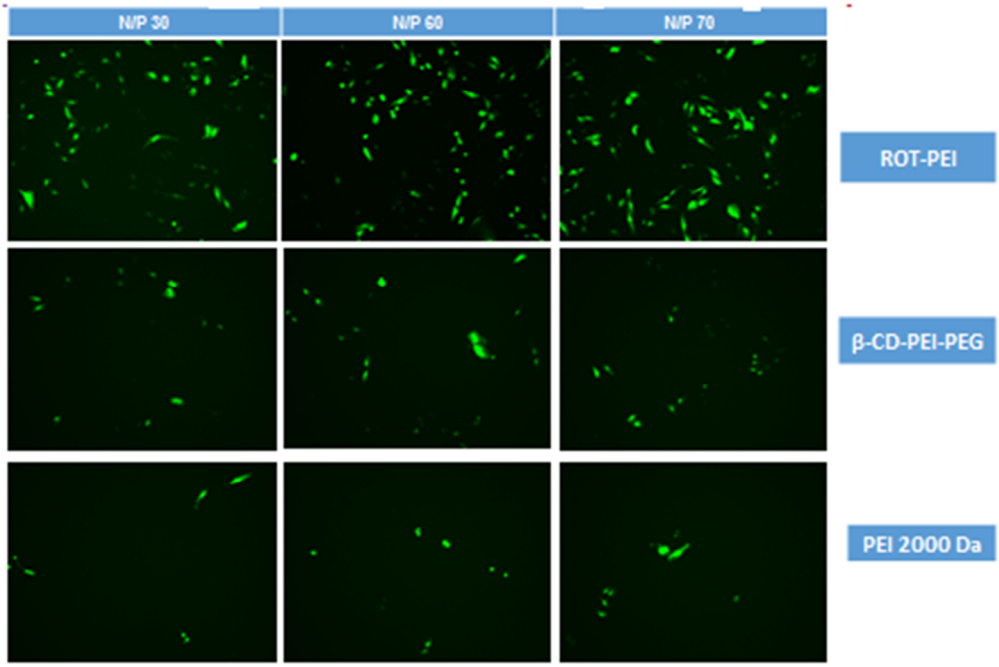

Figure 23. *Transfection of HeLa cells with reporter gene eGFP by non-viral vector/pCS2+MT-Luc polyplexes .*

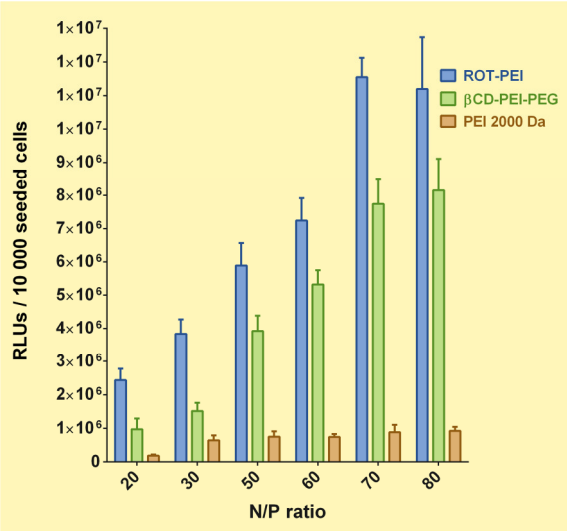

Figure 24. *Quantification of transfection ability of polyplexes, carrying Luciferase gene (The results are given as relative light units (RLUs) per 10 000 seeded cells).*

D. Biosynthesis and characterization of exopolysaccharides (EPS) from lactic acid bacteria, as precursors for non-viral vectors used in gene therapy

Nowadays, due to an increased awareness on environmental problems, it has been developed an interest towards biopolymers, in order to develop environmentally friendly materials suited for high performance applications and for their traditional uses.

The trend of orientation towards biopolymers and to design innovative products has led to a global resurgence of interdisciplinary research on *bacterial exopolysaccharides* (EPS). The inherent bioavailability and the non-toxic nature of EPS resulted in their use in many medical applications such as scaffolds in tissue engineering, systems for controlled release of drugs[31] and many others. These biopolymers include, generally, capsular exopolysaccharides or a viscous substance form.[32]

EPS with precise composition and low polydispersity index could be adequate functionalized to work as non-viral vectors for gene therapy.

D.1. EPS biosynthesis from lactic acid bacteria

EPS extracellular biosynthesis by lactic acid bacteria (LAB) fermentation was considered of interest for this project due to their structural and functional diversity and to their valuable effects. Factors influencing the EPS biosynthesis are the culture medium composition, the incubation conditions, such as the carbon and nitrogen source type, incubation time, agitation speed and incubation temperature.

Fermentation condition

We used only natural compounds for the culture medium compositions. The culture medium imitates the characteristic culture medium used for lactic acid bacteria

growth, with the following composition: 150 g/L commercial sugar, 30 g/L yeast extract, 10 g/L milk powder, 0.05 g/L manganese sulphate and 0.2 g/L magnesium sulphate. The culture medium was sterilized 20 minutes at 120°C, inoculated with 10% of 48 hours fresh inoculums ($A_{600\ nm}$=0.5) and incubated at 33°C, 48 hours. At the end of the fermentations process, the enzymatic inactivation of culture medium was made after.[33] This novel culture medium offers the possibilities to acquire a highest amount of exopolysaccharides obtained until now (**26.6 g** of freeze-dried exopolysaccharides/L culture medium) by using natural components instead of synthetic one for the fermentation processes.

D.2. EPS extraction and purification

First, all the proteins and cells were removed by precipitation with 20% trichloroacetic acid (TCA) and centrifuged 10 min at 4°C and 10.000 rpm (Beckman Coulter Allegra® X-22). The EPS precipitation and separation from culture medium was made following Tayuan A. et al.[34] protocol. The EPS were washed 3 times with chilled ethanol, re-dissolved in DDW and dialyzed (14.000 Da cut-off) against distilled water for 3 days at room temperature. For the gravimetric quantification, the EPS suspended in DDW was subjected to freeze-dryer process, in an ALPHA 2-4 LD Plus Freeze-Dryer, and the result was expressed as polymer dry mass in one litre of culture medium.[35]

D.3. Physico-chemical characterizations of EPS

FTIR analysis of purified EPS produced by *Weissella confusa* in natural culture medium FTIR spectra for EPS was compared with that of pure dextran and there were recorded in KBr pellet, using a Bruker Vertex 70 spectrometer and the (Figure 25).

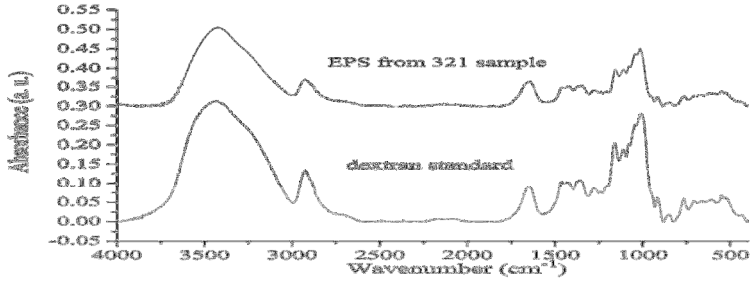

Figure 25. *FTIR spectra of: pure dextran, Mw=40000 and purified EPS produced by Weissella confusa in natural culture medium.*

The characteristics bands at 2926 cm^{-1} for EPS sample and 2925 cm^{-1} for dextran were detected.[36] The presence of the medium signals at 1668 and 1655 cm^{-1} for EPS and dextran, respectively, represent the bending vibration of C-OH groups of glucopyranosyl unit[37] which suggest that the samples are saccharides. Peaks around

1458 and 1342 cm^{-1} were attributed to the asymmetric deformation of C-H bond, confirming the polysaccharide nature of the compounds.[38] The presence of α-anomeric configuration and chair conformation of the glucopyranose units were confirmed by the presence of bands at 843 cm^{-1} for EPS sample and 845 cm^{-1} for dextran.[39] Taken into account of all the similarities between the two spectra (EPS sample and dextran with *Mw*=40.000), we can assign a dextran structure for EPS sample biosynthesized by *W. confusa* in a natural culture medium.

^{1}H and H,C HSQC spectra show the characteristic signals of an exopolysaccharide (Figure 26). Based on previously reported data (Chen Y. et al., 2013) it was deduced that the exopolysaccharide produced by *W. confusa* was dextran.

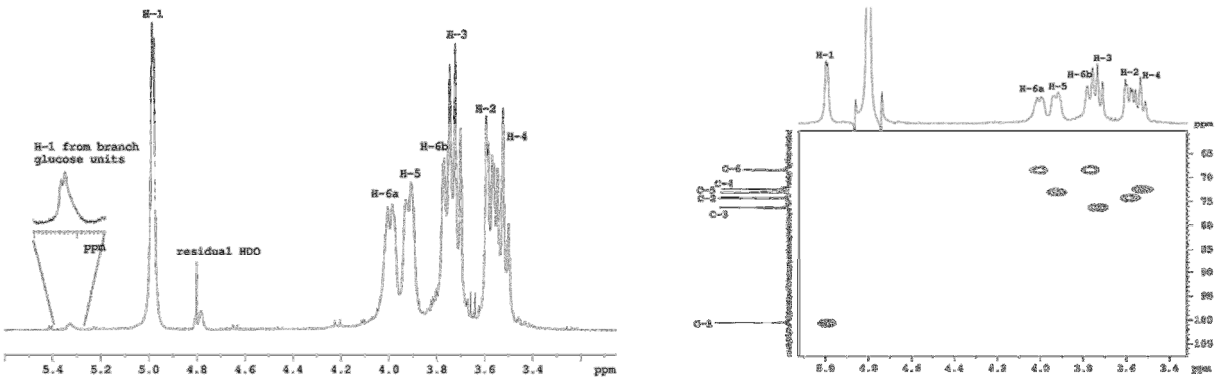

A) **B)**

Figure 26. *NMR spectra of EPS sample produced by Weissella confusa, recorded in D_2O.* ***A)*** *^{1}H NMR spectrum,* ***B)*** *H,C HSQC spectrum.*

For quantitative monosaccharide analysis, hydrolysis of the purified EPS was needed (Tayuan A. et al., 2011). The HPLC analyses were carried out using a Perkin Elmer HPLC system with a Flexar Refractive Index LC Detector. The results (Figure 27) indicated that the glucose was the only monosaccharide of the EPS polymer.

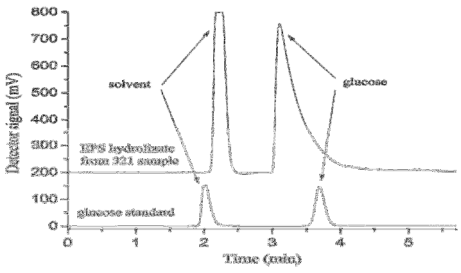

Figure 27. *HPLC chromatograms for glucose standard and hydrolysed EPS sample produced by W. confusa strain fermentation in natural culture medium.*

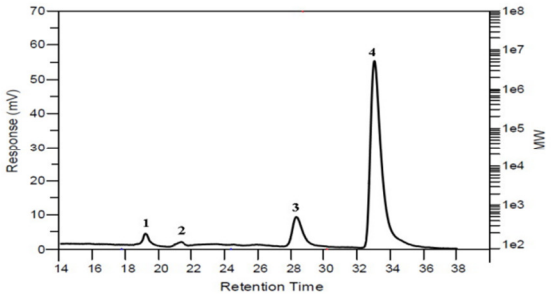

Figure 28. *GPC curve of EPS produced by W. confusa strain in a natural culture medium.*

The gel permeation chromatography (GPC) measurements (Figure 28) were carried out on a device from Polymer Laboratories System (PL-GPC 120, Varian) instrument equipped with refractive index detector. As expected (Figure 4), four fractions, ranging from 10^2 and up to 10^6, were obtained after gel permeation chromatography. High molecular weight (HMW) material $\boldsymbol{M_w}$=1.6 × 10^7 and 3.3 × 10^5 g/mol, respectively include fraction 1 and 2, while low molecular weight (LMW 4.4 × 10^2 and 1.6 × 10^2 g/mol, respectively) consist of fraction 3 and 4. A small polydispersity index of each fraction can be observed, meaning that each fraction is nearly monodisperse (fraction 1 - 1.29 PD; fraction 2 – 1.0 PD, fraction 3 – 1.18 PD). It is well known that the best controlled synthetic polymers have PD of 1.02 to 1.10 and step polymerization reactions yield a PD of around 2.0.[40]

The TGA, DTG and DSC measurements were performed on a Maia F3 200 DSC device (Netzsch, Germany). By comparing the degradation profile of EPS sample biosynthesized by *W. confusa* strain with that of pure dextran (Figure 29A) it can be noticed that the EPS sample degradation presented a similar behavior to that of dextran.[41] It may be observed from the second DSC heating curves of EPS sample and dextran (Figure 29B), that the dextran exhibits a glass transition temperature domain (T_g) at 220°C, as previously described in literature.[42]

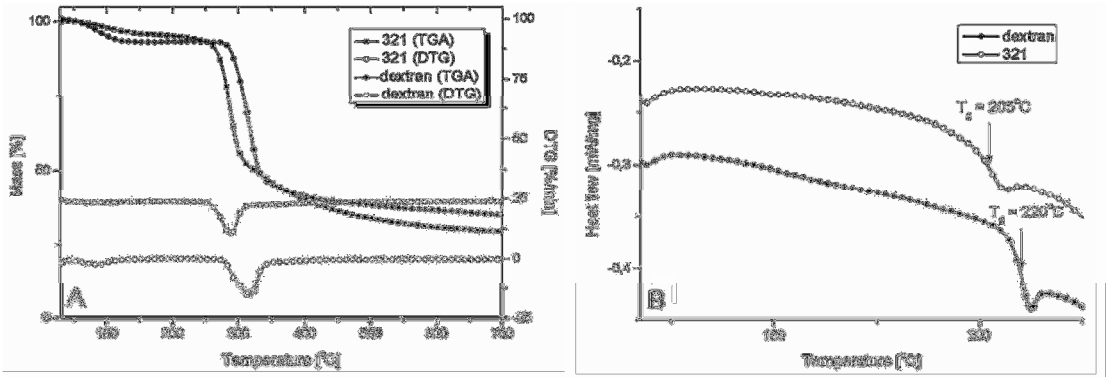

Figure 29. *TGA and DSC analysis for EPS sample extracted from the natural culture medium inoculated with W. confusa lactic acid bacteria and pure dextran (Mn 40000).*

The EPS produced by *Weissella confusa* strain exhibited a lower T_g domain at 205°C. This aspect may be explained by *Weissella confusa strain* producing a dextran with higher segmental chain mobility, probably due to a more amorphous structure.

Conclusions:

- Taking into account the results from FTIR, ^{1}H-NMR, ^{13}C-NMR, HSQC, HPLC and TGA/DTA analysis, the EPS extracted from the fermentative culture medium have a dextran structure, with 100% glucose composition.

- The high molecular weight detected by GPC analysis, classifies the EPS produced by *W. confusa* as a suitable candidate product for medical applications.
- Taking into account the higher amount of EPS obtained by fermentation process (**26.6 g** of freeze-dried exopolysaccharides/L culture medium) and the natural culture medium compositions, this compound is obtained by an inexpensive procedure in a very short time and it can be attributed many applications.
- The natural composition of culture medium is proper for obtaining pure EPS used in pharmaceutical field.
- The obtained EPS structure can be suitable for functionalization in order to obtain a new class of transfection core.

E. The desing and development of an equipment for the synthesis of hydroxyapatite (nano)particles in the presence of biomacromolecules

During the stage 2013 of the project, a patent pending was subjected on a practical procedure to control he characteristics of the hydroxyapatite particles synthesized in the presence of biomacromolecules, as templates. The patent pending was registered at OSIM-București with the number A00710 / 27.09.2013. In the 2016 stage, an equipment was designed, developed and tested, for the control of the synthesis of hydroxyapatite particles in electric field, in capacitive regime. The new patent pending was also registered to OSIM- București, with the number A00615 / 07.09. 2016. Figures 30 and 31 describe the equipment parts.

The problem solved by the patented invention consists in the elimination of the secondary effects induced by the direct contact of the aqueous synthesis milieu with the electrodes. The equipment allows to control the crystallinity degree, the dimensions, the morphology and the phase distribution of the synthesized calcium-deficient hydroxyapatite. The inventive solution consists in:

- the separation of the reaction milieu and the electrodes by an impermeable and dielectric barrier;
- the number, form and placement geometry of the electrodes that act as plates of the capacitive system;
- the method of reduction of the ripple of high voltage sources;
- the control diagram of the electric potential time evolution (value, polarity, frequency, harmonic or disharmonic form).

The equipment is composed by:

- the reaction vessel (1);
- the electric circuits, including the electrods (3, 3');
- the high and low voltage sources (8 and 6, 6');

- an electronic circuit for ground potential rise of the electric ground of the electronic command blocks, against the null potential of the capacitive system (9);
- the digital system for the time evolution of the working potential of the electrodes (7);
- four systems to assist the synthesis of hydroxyapatite:
    - a protection system against electrostatic discharge (10);
    - a thermostatic system to control the temperature of the liquid in the reaction vessel (11);
    - a dosing system for the necessary reagents (12);
    - a mixing / recirculation system for the content of the reaction vessel (13).

The equipment was used to produce collagen – hydroxyapatite mixt scaffolds for cells culturing and transfecting.

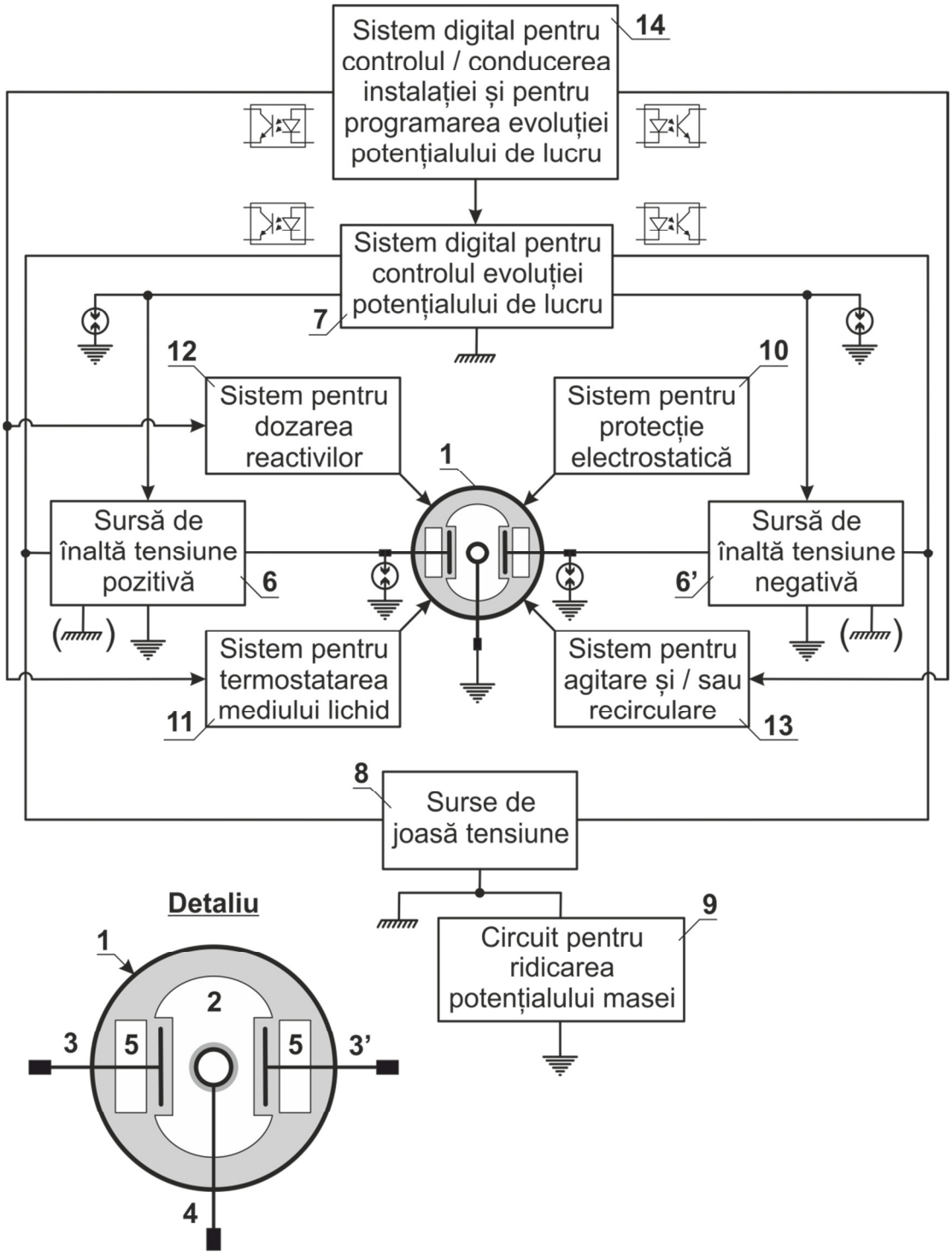

Figure 30. *The block scheme of the patented equipment.*

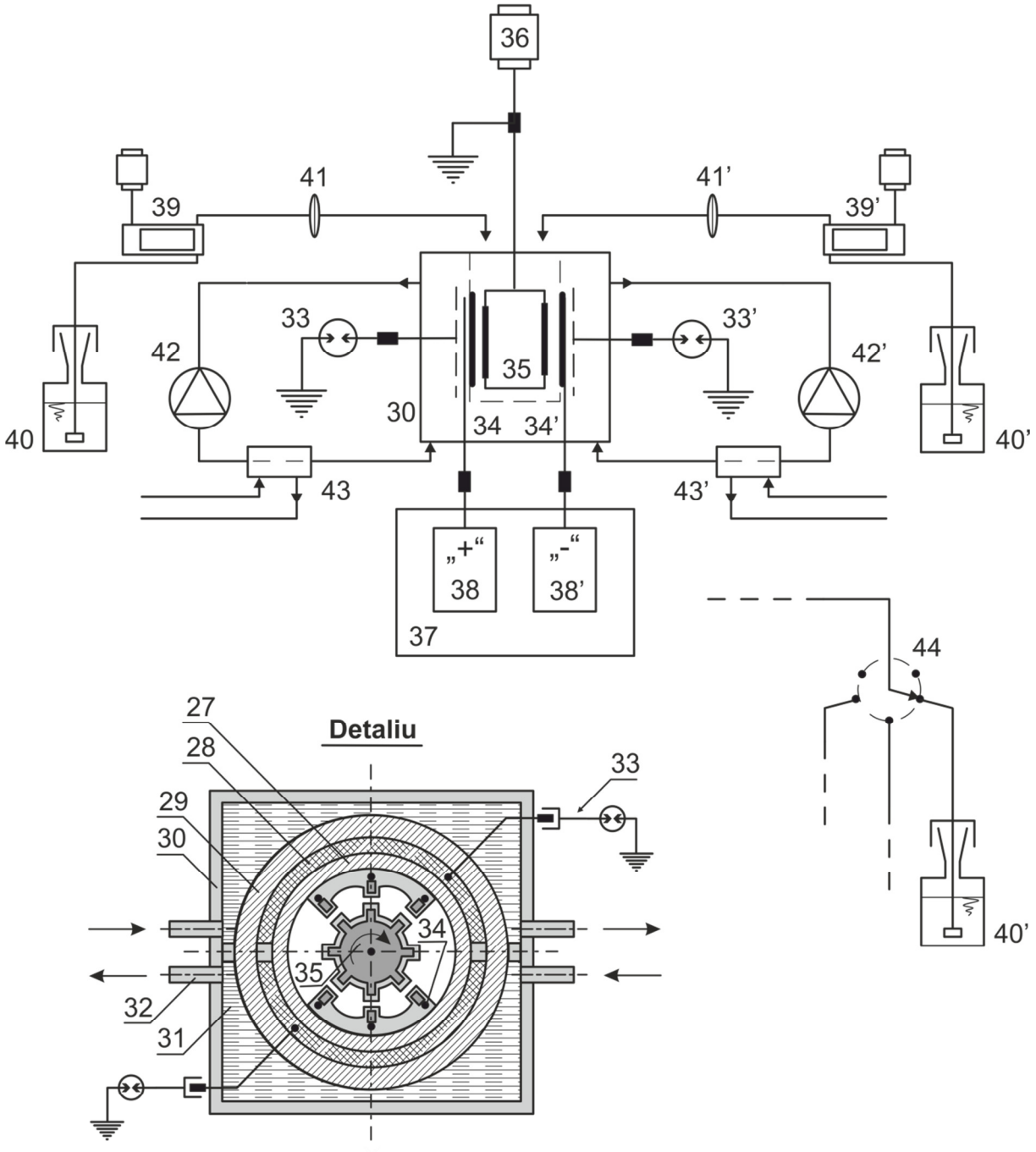

Figura 31. *The functional scheme of the patented equipment.*

Objective 2'. Drug delivery systems

2'.1. Smart nanoparticles based on Pullulan-g-poly(N-isopropylacrylamide) for controlled delivery of indomethacin

In the last ten years, researchers have been deeply involved in smart drug delivery systems that are able to release the therapeutic payload "on demand".[43]

Nanoscale drug delivery vehicles formulated from biocompatible and biodegradable thermoresponsive polymers represent a promising approach to lipophilic drug delivery. Poly(N-isopropylacrylamide) (pNIPAM), due to its special property, has been used in this study for synthesis of copolymers with pullulan and then for stimuli-responsive polymeric micelles for drug delivery purpose. pNIPAM exhibits a reversible phase transition in aqueous solution at about 32^{o}C, which is known to be the lower critical solution temperature (LCST).[44] The micelles can be constructed when the temperature is raised above the LCST of the block copolymers containing pNIPAM, where pNIPAM forms the hydrophobic core or by nanoprecipitation below LCST in the presence of a hydrophobic drug. The block copolymers compose the so-called thermosensitive micelle-forming polymers. In order to develop new nanoparticulate thermoresponsive carrier with good entrapment efficiency for lipophilic drugs, double hydrophilic thermo-responsive pullulan-g-poly(N-isopropylacrylamide) (P-g-pNIPAM) copolymers with two different molecular weight of thermosensitive grafts were designed and synthesized and used for preparation of indomethacin-loaded nanoparticles by dialysis and nanoprecipitation method. The polymers form aggregates in aqueous solution at a concentration of 10 g/L, above their critical aggregation concentration (3.36 g/L) and below the lower critical solution temperature (LCST). FT-IR spectra proved that the main driven force for the aggregation was the hydrogen bonding between indomethacin and the pNIPAM side chains of copolymer. After indomethacin loading, nanoparticles with compact and uniform structure were formed below the LCST. The effects of copolymer composition, concentration, and the feed polymer/drug ratio on the particle size, drug loading content (DLC) and entrapment efficiency (EE) were investigated. DLC increased with drug feeding, reaching a maximum value of 40 % at the ratios of 1/1. The size of IND-loaded P-g-pNIPAM nanoparticles decreased with the increase of molecular weight of thermoresponsive fragments, the loading amount of drug and the concentration of copolymer. Smaller particles (145 nm) with narrower size distribution were obtained from polymer with a higher molecular weight of pNIPAM grafts. The drug entrapment efficiency was up to 80 % when the weight ratio of IND/polymer was 1/1 and for a 10 g/L polymer concentration. The indomethacin release rate from nanoparticles was influenced by temperature, because of the dissociation of the hydrogen bonds at high temperatures, the degree of drug loading, and the pH of the release media.

2'.2. Inclusion complexes of propiconazole nitrate with substituted β-cyclodextrins. Synthesis and characterization

The study is driven by the fact that fungal infections are an important health issue fueled by the recent advancements in medical care, while azoles, diazoles and triazoles, like PCZH-NO_3, are the largest and most widely used class of antifungal agents. The first main objective of this study is to report the synthesis and characterization of the inclusion complexes formed by propiconazole nitrate (PCZH-NO_3) with sulphobuthyl ether β-cyclodextrin (SBE7-β-CD, Captisol), sulfated β-cyclodextrin (β-CD-SNa) and monochlorotriazinyl-β-CD (MCT-β-CD) (Figure 32). The second main objective is to biologically test inclusion complexes. The obtained results intend to confirm the supramolecular compounds formation, to establish the combination ratio and the relation between structure and stability and to assess the antifungal activity and the cytotoxicity of the inclusion complexes.[45,46]

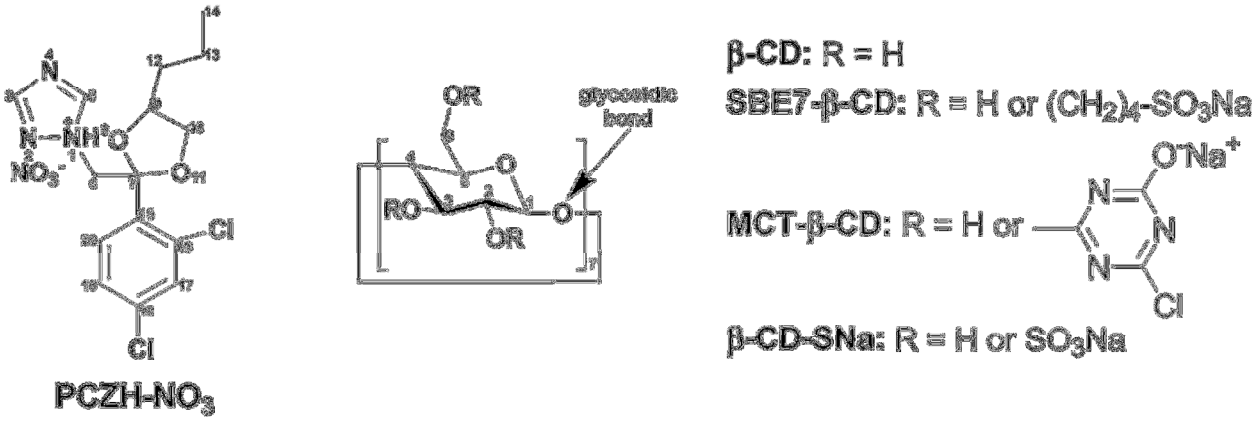

Figure 32. *The chemical structures of PCZH-NO3, β-CD and its derivatives used in this study.*

The inclusion complexes of different cyclodextrins with PCZH-NO_3 were prepared by *freeze-drying* method, using 1/1 v/v water/ methanol solutions, of, SBE7-β-CD, MCT-β-CD, β-CD-SNa and PCZH-NO_3 in a 1/1 molar ratio. The solution mixtures were steered until turbidity appears and then were subjected to lyophilization. Inclusion complexes are presented in the form of white powder, with yields close to 100% as demonstrated by DSC studies.[47]

The formation of the inclusion complexes were confirmed by NMR experiments. Due to the complexity of the system containing cyclodextrin random substituted (stereoisomers) the formation of the inclusion complexes was deduced from the chemical shift changes of the PCZH-NO_3 aromatic protons. ^{1}H-NMR spectra of the inclusion complexes showed changes in resonance frequencies for the aromatic protons of both the triazole and 2,4-diclorophenyl group. The chemical shifts variation were attributed the perturbation of these protons due to the complex formation. The formation

of the inclusion complexes was further confirmed from ROESY experiments. The ROESY spectra of the MCT-b-CD/PCZH-NO_3 and SBE7-b-CD/PCZH-NO_3 inclusion complexes showed intermolecular NOE cross-peaks between triazole and 2,4-diclorophenyl rings from PCZH-NO_3 and the protons from the inner cavity of the CD derivatives (Figure 33). Thus, it might be concluded that two types of inclusion complexes simultaneously exist in the solution: a first type, when the 2,4-diclorophenyl ring enters into the CD cavities, and a second type, when the triazole ring is inside the CD cavities. These data suggest a multiple conformers coexistence, which is a confirmation of the previous theoretical results.[12]

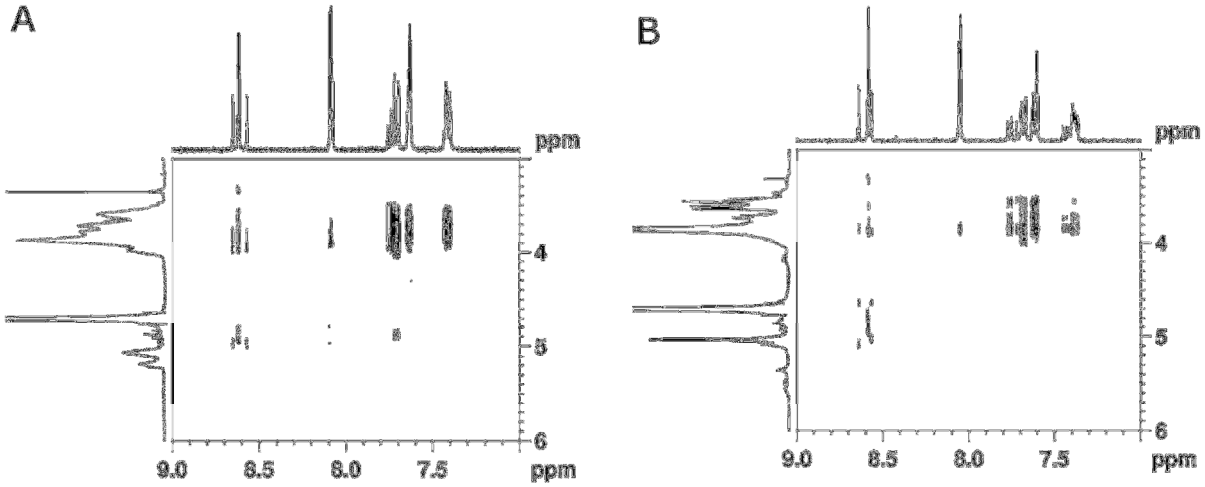

Figure 33. *ROESY spectra of (A) SBE7-b-CD/PCZH-NO_3 and (B) MCT-b-CD/PCZH-NO_3 inclusion complexes.*

The 2D ROESY spectrum for β-CD-SNa/PCZH-NO_3 was not conclusive, possibly because the $–SO_3^-$ radicals are directly linked to the hydroxylic oxygen of the cyclodextrin.

The association constants (Ka) of the inclusion complexes were determined by ^{1}H-NMR titration of protonated propiconazole nitrate with each cyclodextrin using the chemical shifts of the 2,4-dichlorophenyl protons and by applying the NMR version of the Benesi-Hildebrand equation. In this experiment, the ^{1}H-NMR spectra of different mixtures of PCZH-NO_3 and cyclodextrins were obtained by keeping the concentration of PCZH-NO_3 constant and varying the concentrations of the cyclodextrins. The double-reciprocal plots of the NMR version of the Benesi-Hildebrand equation gave straight lines, confirming the 1:1 stoichiometry of the inclusion complexes. [48] The values of the association constants were 1050 and 250 M^{-1} for SBE7-b-CD and MCT-b-CD, respectively.

The antifungal activity of the complexes was assessed on 20 *Candida* spp. clinical isolates (10 *Candida albicans* + 10 *C. glabrata*) growing as planktonic phase. The *in vitro* susceptibility testing was performed following the EUCAST EDef 7.2 guidelines.[49]

Against planktonic yeasts, all four complexes exhibited antifungal activity at low and similar concentrations (Figure 34A). The experiments showed that, in the majority of cases, the minimal inhibitory concentrations (MIC) were in agreement with differences confined within the accepted ± 1 log2 dilution interval.[50] This suggested that the nature of the cyclodextrin does not significantly influence the *in vitro* behavior of PCZH-NO_3 towards fungal cells.

To assess the cytotoxicity, the CellTiter 96®AQueous One Solution Cell Proliferation Assay (Promega) was performed on normal human dermal fibroblasts - NHDF (PromoCell) by following the protocol recommended by the manufacturer.[51] The nonlinear regression curves (Figure 34B) showed the inclusion complex of PCZH-NO_3 with the parental β-CD to be more toxic than the complexes with the three β-CD derivatives. The half maximal inhibitory concentrations (IC_{50}) were two to three orders of magnitude higher than the concentrations required for antifungal activity.

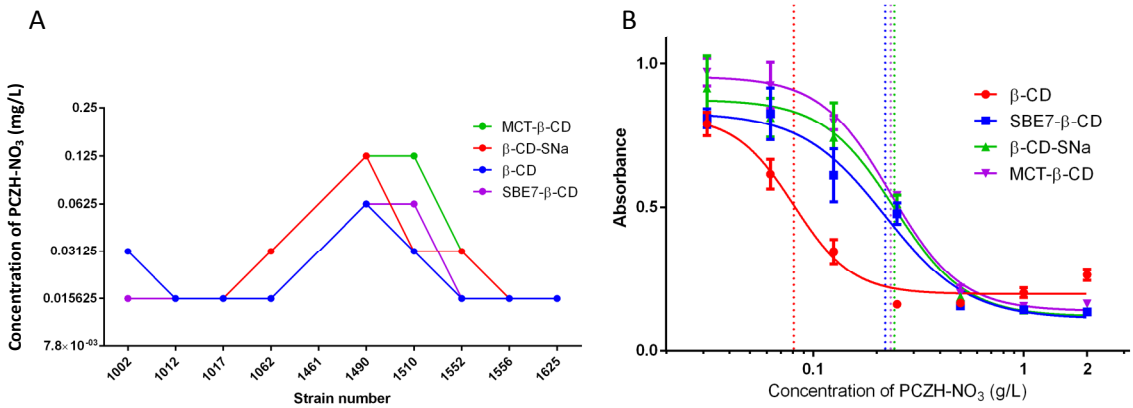

Figure 34. *The biological activity of the inclusion complexes.*
A: *MIC agreement between the four tested inclusion complexes based on PCZH-NO_3 and β-CD or its derivatives against C. albicans isolates;* ***B:*** *The cytotoxicity of the four inclusion complexes based on PCZH-NO_3 and β-CD or its derivatives - nonlinear fit of the dose response curves. The dotted lines indicate the IC_{50} values.*

Conclusions

The ^{1}H- and 2D ROESY NMR studies demonstrated the formation of host-guest inclusion complexes between protonated propiconazole nitrate and three b-cyclodextrin derivatives.

NMR titration-measured association constant values highlight that PCZH-NO_3 form the most stable inclusion complex with SBE7-b-CD, probably due to the interactions of the dioxolanyl and triazolic cycles with the glycosidic oxygens or the $-SO_3^-$ groups of the cyclodextrin. Additionally, the titration experiments data were furnish the ratio complexation between the two components, which is 1:1 for all cases.

The lack of significant differences in the antifungal susceptibility tests and the differences in cytotoxicity between the complex with the parental β-CD and the

complexes with β-CD derivatives suggest that the type of cyclodextrin may be more important for the interaction of the compounds with the infected host than it is for the actual antifungal activity.

2'.3. New hybrid materials based on layered double hydroxides (LDHs) as drug delivery systems

Layered double hydroxides (LDHs) represent a class of materials characterized by layered structure, in which the lamellae are positively charged and stability of the structure is ensured by the anions which connects adjacent layers in an electrostatic way.[52] LDHs are biocompatible materials, and can be explored as matrix for biomolecules/drugs storage and controlled release systems.[53–55] It was reported that the intercalation of the drug molecules in the layered double hydroxides matrix do not only reduces the negative effects of the drug, but in some cases, there is an increase in drug solubility.[56] Tramadol hydrochloride (TrH) is an opioid used to treat moderate to moderately severe pain. TrH is fast processed by the human body and therapeutic effect is lost in only four to approximately six hours and for maintain its effect must be administred five daily doses. Therefore, several systems for controlled release of TrH have been developed using montmorillonite composites, ethyl cellulose microparticles, ion-exchange fiber etc.[57]

In this context, we focused on obtaining new hybrid materials based on layered double hydroxides (LDHs) able to act as effective drug delivery systems. Tramadol hydrochloride (TrH) has been chosen as model drugs, being intercalated in a ZnAl nitrate LDH matrix by anionic exchange method. TrH was used in different amounts 0.1, 0.4 and 0.8 g for each 2 g ZnAlLDH.[58]

The XRD diffractograms (Figure 35) shows symmetric reflections of the basal (003), (006), (009) and (110) planes, characteristic to layered materials. According to the XRD data, the intercalation of the TrH molecule it was carried out only in the case of ZnAlLDH_TrH 0.4 and ZnAlLDH_TrH 0.8 samples, when occurs an increase of the interlayer distance from 8.74 Å for ZnAlLDH to 9.29 Å and 11.55 Å for the hybrid compounds. In the case of ZnAlLDH_TrH 0.1 intercalation has not been performed (there is no shifting in XRD diffractogram), but occurred the TrH adsorption only on the LDHs surface.

FT-IR and Raman spectroscopy gives us information about the nature of the ions present between layers. In the FT-IR spectra of hybrid materials can be observed characteristic absorption bands to LDH matrix with a number of characteristic vibration bands of TrH (Figure 36).

EDX analysis confirms the presence in the hybrid compound of TrH molecules, by increasing the carbon percentage and by the chlorine presence from TrH molecules The

SEM micrograph of the ZnAlLDH shows a porous structure with particles of regular hexagonal shape in the size range of 1-1.5 µm (Figure 37).

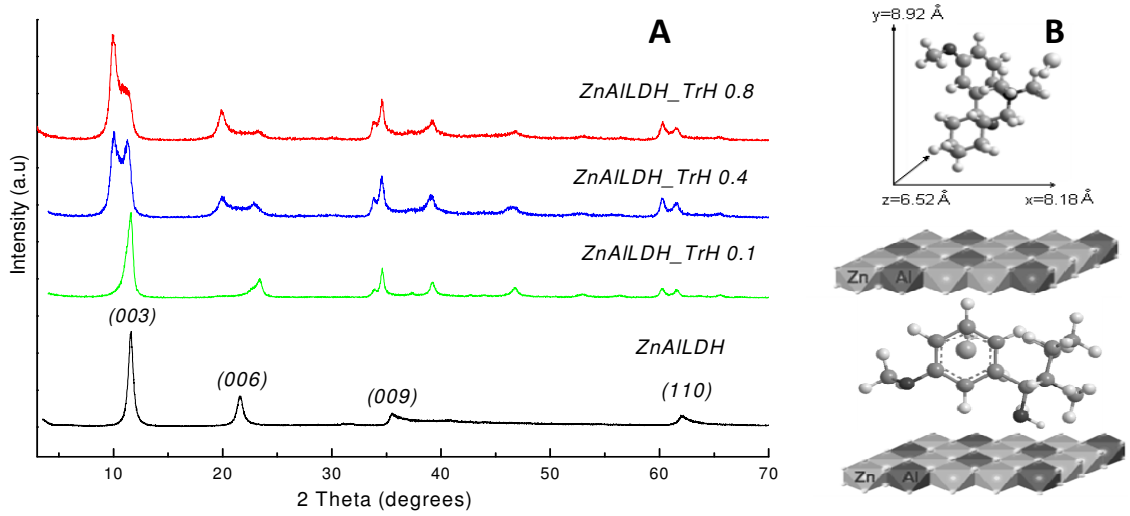

Figure 35. (A) *XRD patterns of ZnAlLDH, ZnAlLDH_TrH 0.1, ZnAlLDH_TrH 0.4 and ZnAlLDH_TrH 0.8;* ***(B)*** *Three-dimensional size of TrH and proposed model for the orientation of the TrH in the interlayer space.*

The obtained results point out the presence of the TmH in the interlamelar space in the case of ZnAlLDH_TrH 0.4 and ZnAlLDH_TrH 0.8 when a larger amount of TrH was used for the ion exchange. The FTIR and RAMAN spectra points out the absence of vibration bands characteristic to nitrate ions, which also confirms their replacement with TrH anions. In the other cases was observed the partial TmH intercalation and a significant absorption on the surface of ZnAlLDH.

In conclusion, this study suggests that TmH can be intercalated into ZnAlLDH, and the new hybrid materials could open interesting perspectives for obtaining the drug reservoirs and controlled release systems.

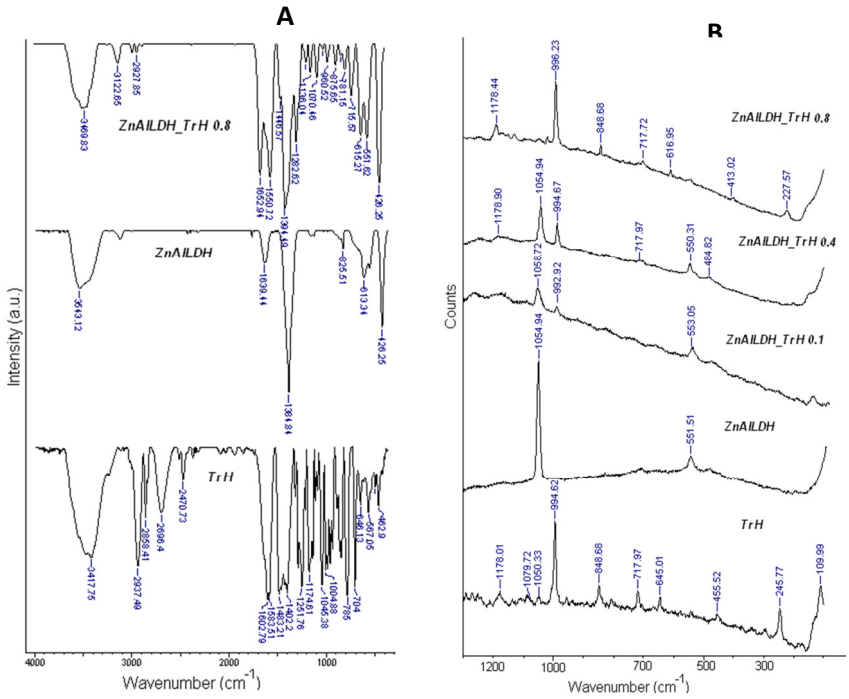

Figure 36. (A) *FT-IR and* ***(B)*** *RAMAN spectra recorded for indicated samples*

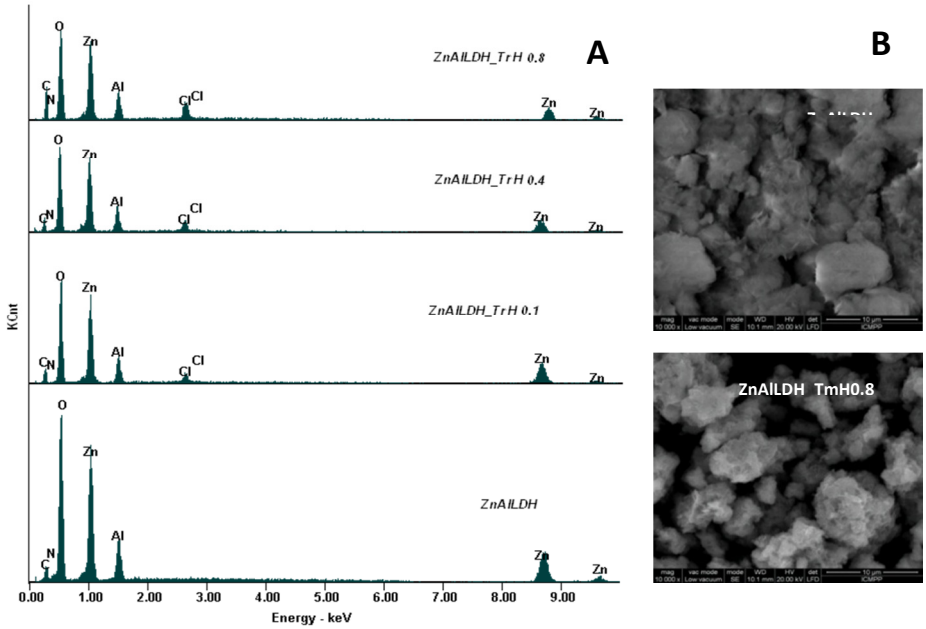

Figure 37. (A) *EDX spectra of ZnAlLDH, ZnAlLDH_TrH 0.1, ZnAlLDH_TrH0.4 and ZnAlLDH_TrH0.8;*
(B) *SEM micrograph for ZnAlLDH and ZnAlLDH_TrH0.8*

Objective 3. The evaluation for transfection of structured composites loaded with polyplexes

3.1. The evaluation for transfection of structured composites loaded with polyplexes

Besides nanotechnology and natural biomaterials (as was mentioned at Objective 2), another important strategy for optimizing the structure of non-viral systems and the delivery mode of DNA carried by the non-viral systems, involves the **integration of gene delivery vectors into scaffolds (**considering their unique properties such as biodegradability, biocompatibility, and controlled release, emphasizing the lowering of risk of toxicity at high-dose applications). Also, scaffold-mediated non-viral gene delivery holds the advantage to function as a gene reservoir able to generate a sustained expression of a particular protein in the cells in the vicinity *in vitro* and *in vivo*, after implantation.

In this context, efficient and controlled gene delivery from biodegradable materials was proved to stimulate cellular processes that lead to tissue regeneration.[59–61] Scaffold mediated gene delivery can provide a fundamental tool to promote sustained (prolonged), localized transgene expression, which can be employed to direct cellular processes for numerous tissue engineering applications. In comparison with the most short half-lives of biological factors (related to protein degradation or diffusion from the defect site), DNA retains its structural and functional integrity in many solvents, this combination of both approaches from gene delivery and tissue engineering offering the potential to bypass the use of expensive and relatively inefficient growth factor supplementation strategies to augment cell behavior. This strategy allows overcoming extracellular barriers to efficient plasmid delivery, also avoiding laborious synthesis steps (required to achieve the multifunctionality related to these barriers surpassing).

3D scaffolds based on natural polymers and condensed DNA inclusion in the matrix was found to be recommended in order to achieve high efficacy and safe profile for gene therapy.[62–65] The main arguments are:

1. The sustained release of plasmids (pDNA) can be modulated by tailoring the scaffold chemistry, topology, architecture through processing parameters control.
2. Scaffolds based on natural polymer components are functionally superior providing a biomimetic extracellular matrix and informational signaling molecules (such as gelatin, collagen, and glycosaminoglycan (GAG)), increased biocompatibility and biodegradability. To control degradability and to avoid the disadvantage of such materials own inherently poor mechanical properties and processability a combination of biopolymers with synthetic polymers is a better strategy for scaffold construction.

3. Cell culture studies demonstrated that collagen matrices containing condensed pDNA (LIP or PEI) are effective in comparison to naked pDNA and pDNA matrices (which use is also related to some cytotoxicity due to the high dose).
4. Such systems offer protection from rapid degradation by nucleases (both due to the matrix and DNA condensation).
5. The gene transfer efficiency is increased due to the large surface area provided by the matrix, and increased gene expression in cells migrating into the matrix.

In this context the objectives of the present study were:

a) the examination of the effects of incorporating the Sq-PEI polyplex (Scheme 1) in a hybrid biomimeting macroporous 3D matrix /scaffold for hard tissue regeneration;

b) the comparison with other non-viral complex transfer system based on pDNA/DNA embedded in similar matrices with alternative hyperbranched hybrid bPEI – based condensing agents, having a fullerene (C60) or siloxane core (Figure 38 and 39). According to preliminary data for Sq-PEI, C60-PEI and cD_4^H-PEI N/P ratios of 10,30 and 60, respectively[26,27] were chosen for further investigations on the immobilization effect of these non-viral/DNA complexes to hybrid hydrogels based on biopolymers/synthetic polymers/nanohydroxyapatite. Also, the used non-viral vectors were labelled with fluorescein isothiocyanate (**FITC**), a derivative of fluorescein used in wide-ranging applications, including UV-Vis, fluorescence and flow cytometry.

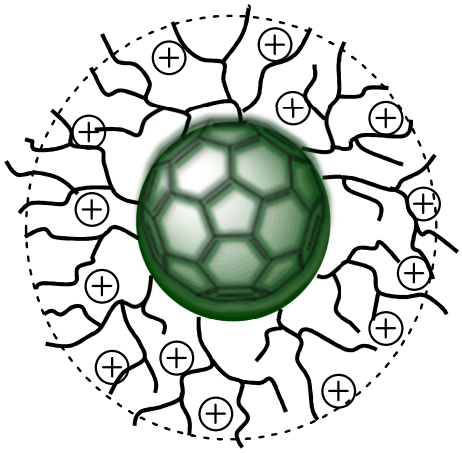

Figure 38. *bPEI based vector with C60 core.*

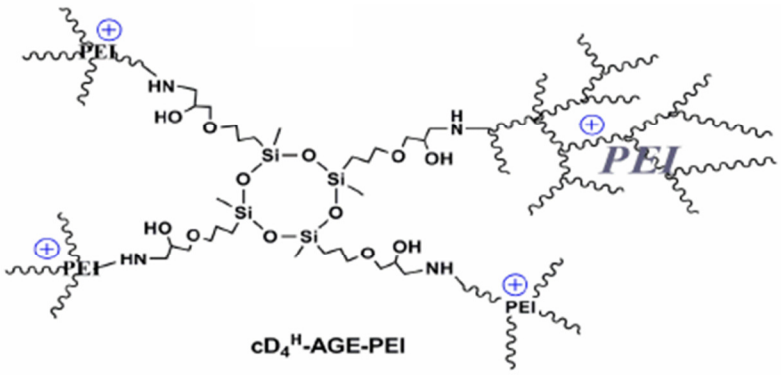

Figure 39. *bPEI based hyperbranched vector with cD_4^H core.*

Non-viral vector loading in hybrid macroporous scaffold. In vitro gene delivery and expression

In this report we have developed complex systems by immobilization of already mentioned polyplexes, to previously synthesized macroporous hybrid scaffolds (2015-

project report), with optimized architecture, pore structure and mechanical strength for bone repair. Envisaging their evaluation for hard tissue regeneration the selected formulation included two biopolymers, main ECM components (protein/atelocollagen and GAG/hyaluronic acid derivative), a poly (ε-caprolactone) derivative (PCL), a synthetic polymer, acting as a cross-linker and degradation rate controller, and nano-hydroxyapatite surface functionalized with linear polyethylenimine (LPEI, 1.8kDa). The surface functionalization and nano-range dimensions of inorganic material favored its uniform distribution in the polymeric matrix, with increased cohesivity and mechanical properties. Cryogelation was selected as a preparative strategy in order to insure the required morphology (interconnected pores with dimensions from 80 µm to ~110 µm) and porosity. Its composition was designed to allow specific interactions with the polyplexes and their components (Figure 40).

The basic formulation was prepared by incubating the scaffold in polyplex aqueous solution at room temperature, for 60 min, followed by lyophilization. To not lower the mechanical resistance a content of 5% genetic material relative to the porous matrix was chosen, while the vector amount was calculated as mentioned before.

For DNA release examination FITC labeled vectors (Sq-bPEI-FITC and C60-bPEI-FITC) were used. For examination of the effect of vector embedding strategy, in the case of C60-bPEI-FITC a first sample was prepared as mentioned, and a second one was prepared by inclusion of the carrier alone in the feed formulation for the cryogel synthesis

Indeed, according SEM observation data, due to the high matrix functionality the polyplex could be immobilized by non-covalent interactions not only at the scaffold surface, but also inner pores (Figure 40). During incubation a clearance of the polyplex dispersion was observed, suggesting that specific interactions developed preferentially between polyplexes and matrix components. For the cryogel including C60-bPEI-FITC in the formulation from starting synthesis it is obvious an increase in pore walls dimension. Particles with dimensions in the range of 500-700 nm uniform embedded in the matrix materials are visible. The bPEI-based materials retention was confirmed also by EDX data (Figure 40).

The mechanism of DNA transfer from the substrate was characterized by examining vector and DNA release from the substrate. To study the release kinetics, hybrid matrices were immersed in water and incubated at 37ºC on a shaker at 100 rpm. At different time points, 100 µl supernatant was separated from the matrices, diluted 100 times and analyzed by fluorescence and UV-VIS methods. In the second case the examination was performed against appropriate blanks containing supernatants from the sample containing only hybrid cryogel without carriers or polyplex. The samples were also evaluated for integrity of the released pDNA (by electrophoresis). At each time point, fresh bidistilled water was replenished.

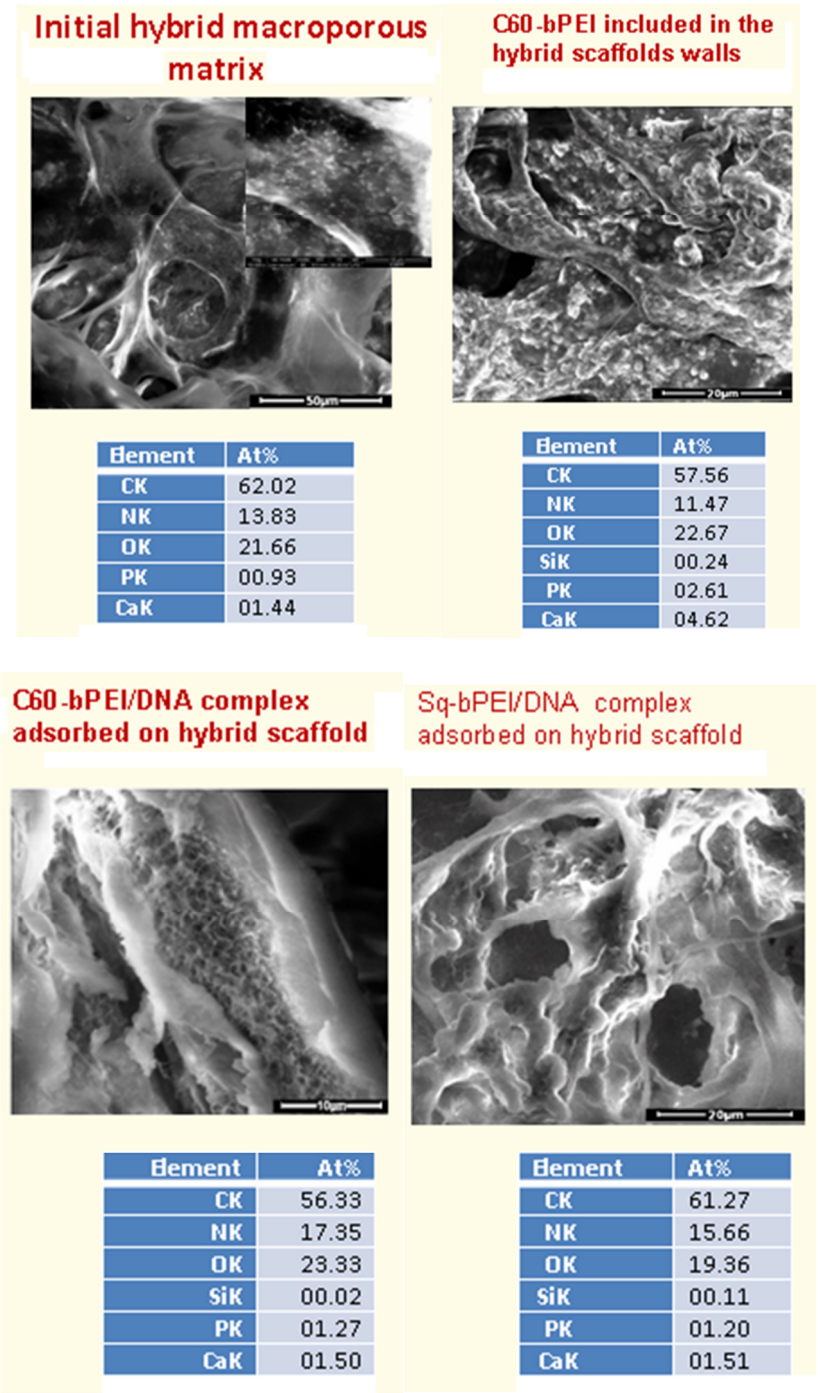

***Figure 40**. SEM micrographs and EDX data confirming polyplex efficient adsorbtion and C60-bPEI-FITC inclusion in the cryogel structure.*

For the system containing hybrid cryogel and Sq-bPEI-FITC /salmon DNA mixture the results are presented in Figure 41. Even if wt:wt ratio of the vector:DNA in this case is 2, in the first 24 h 10 times higher amount of vector than AND is released, suggesting that mostly the free carrier is slightly adsorbed at the matrix surface. The graphs

evidence the maintenance of an elevated concentration of DNA within the matrix microenvironment via sustained release.

The released pDNA was analyzed by gel-electrophoresis for structural integrity (1% agarose, 0.1 mg% ethidium bromide in TES buffer, 100 V, 45 min). No modification was found over the experiment duration.

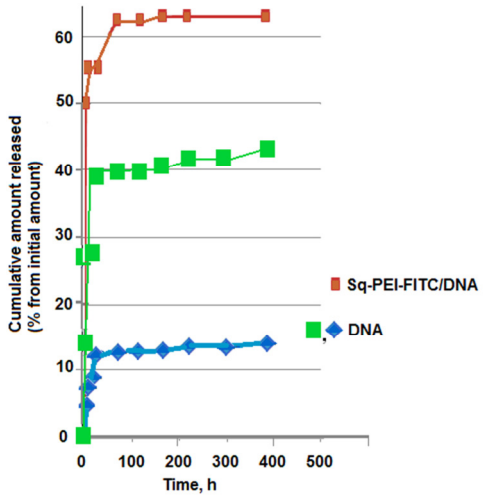

Figure 41. *Quantitative release evaluation of (a) Sq-bPEI-FITC (wt% of total vector amount loaded), (b) salmon DNA (wt% of total DNA amount loaded) and (c) (wt% of total vector and DNA amount loaded) from hybrid matrix.*

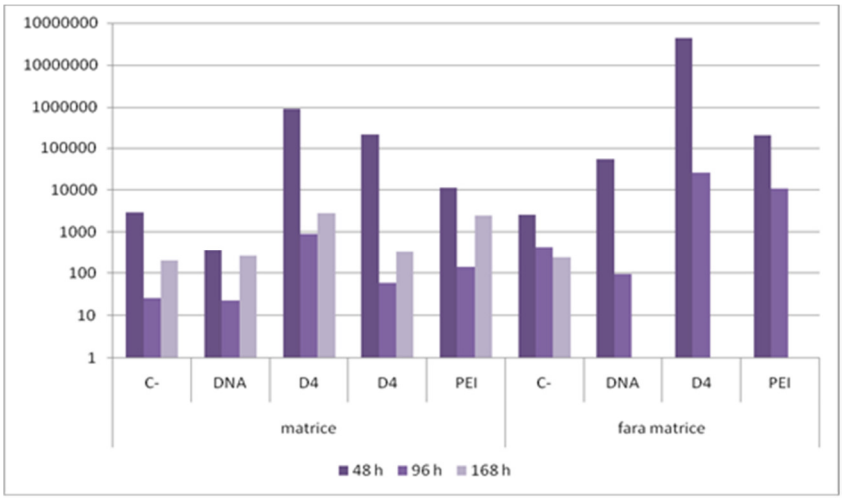

Figure 42. *Transfection efficiency comparatively evaluated over time for different systems; C- control cells (HEK 293T cell line); DNA: cells incubated with naked pDNA; D4: cells incubated with cD_4^H-PEI/ pCMV-luc (N/P=60); PEI: cells incubated with PEI25k/ pCMV-luc (N/P=2).*

Preliminary studies verified that *in vitro* released genetic material exhibited transfection capability. The comparative *in vitro* study of transfection efficiency for polyplex formed by cD4-bPEI with pCMV-luc (N/P=60) comparative with uncomplexed/naked pCMV-luc and even with bPEI (25kDa)/ pCMV-luc polyplex, (N/P=2) embedded or not in the hybrid matrix, evidenced higher gene expression levels for the polyplex cD4-bPEI(1,8 kDa) / pCMV-luc (Figures 42 and 43) in both cases. Prolonged expression (even after 196 h as compared to scaffold free systems with activity limited to 86h) was obtained, at enough good level, for the complex

polyplex/scaffold system without affecting cells. Evaluation of gene expression over time mediated by the hybrid matrices was carried out on HEK 293T cell line.

The experiments confirmed also that the presence of the blank matrices neither hampered the transfection ability of the cells nor had any toxic effects.

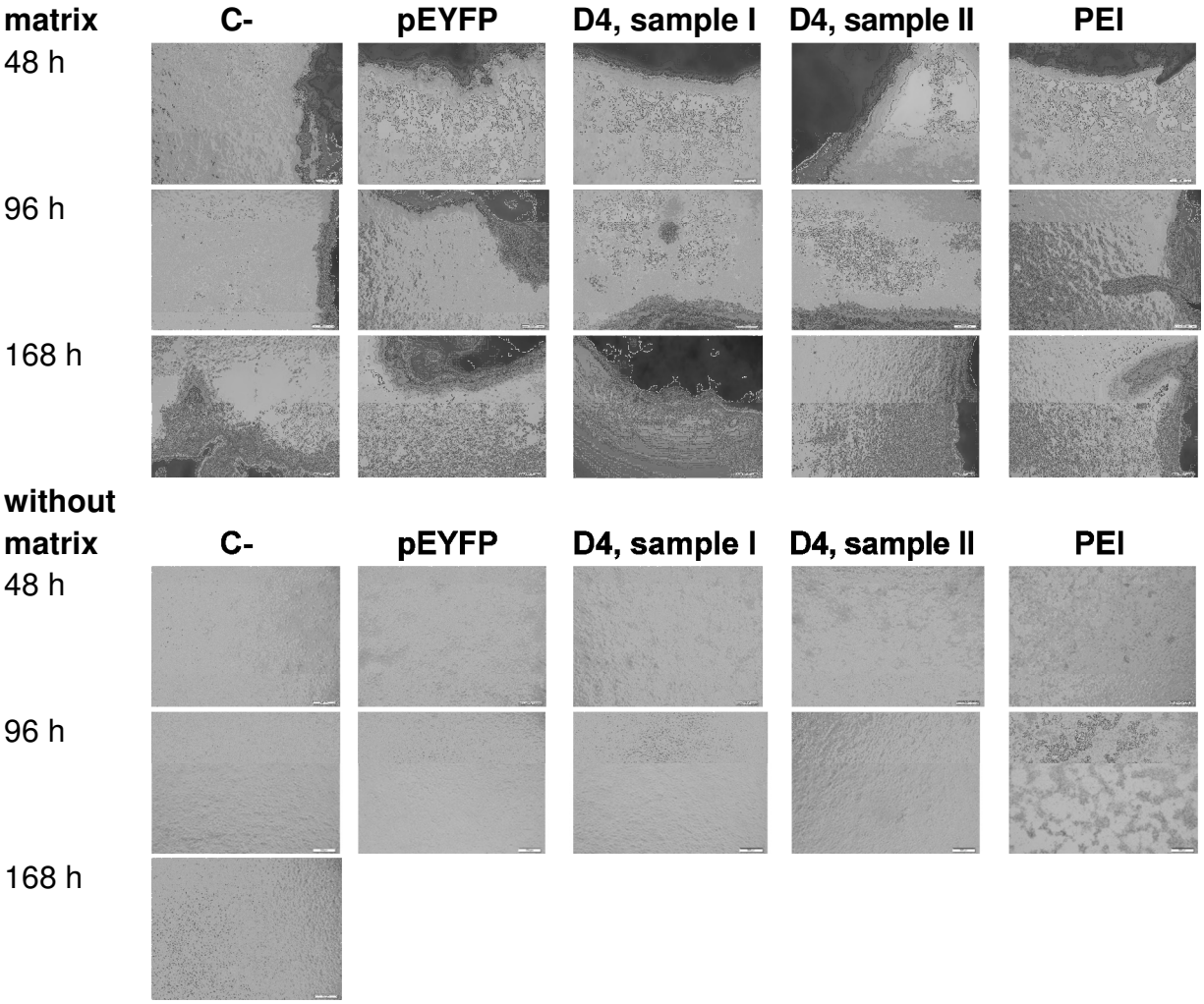

Figure 43. *Cell culture images. Evolution over time for the investigated systems; C: control cells (HEK 293T cell line); pEYFP: cells incubated with naked EYFP plasmid; D4: cells incubated with cD_4^H-PEI/pEYFP (N/P=60); PEI: cells incubated with PEI25k/pEYFP (N/P=2).*

The same matrix but in this case containing C60-PEI immobilized in the walls has been tested to investigate its capacity to deliver the encapsulated polyplexes to the cells cultured in their presence and to test its ability to perform cellular transfection. The polyplexes between C60-PEI immobilized in the matrix's walls and plasmid DNA were formed by hydrating the matrix in water containing plasmid pEYFP (encoding the fluorescent protein YFP) at a concentration so as to obtain a ratio of nitrogen atoms in the polymeric compounds and phosphorus atoms DNA (N/P) of 30.

The ability of matrix to deliver the encapsulated polyplexes and to perform cellular transfection was tested using HEK 293T cells by following the expression of protein encoded by the delivered plasmid. Moreover, the cytotoxicity of degradation products of matrices with loaded polyplexes resulted after their incubation for different periods of time (24h, 48h and 72 h) at 37℃ in DMEM culture medium supplemented with 10% fetal calf serum was tested on HEK 293T cells after exposure for 48 hours to medium containing the degradation products of matrices.

The ability of matrix containing C60-PEI included in the matrix walls to mediate the transfection of plasmid pEYFP (complexed with C60-PEI imobilized in matrix) in HEK 293T cells was tracked using the fluorescence microscopy. Phase contrast images superimposed on the fluorescence fields can be seen in Figure 44. It can be seen a good transfection of cells incubated with free C60-PEI/pEYFP polyplexes at 3 and 6 days of incubation, the expression of fluorescent protein lasting up to 13 days in few cells. When poliplexes were formed between plasmid pEYFP and C60-PEI immobilized in the matrix walls, can be observed that after 3 days of incubation matrix/polyplexes with cells, the polyplexes formed in the matrix are capable of performing transfection in cultured cells incubated in the presence of matrix. This suggests that polyplexes are released from the matrix and are able to induce the expression of fluorescent protein in the cells. The expression of fluorescent protein is observed up to 13 days of incubation between matrix/polyplexes and cells. It may be noted a progressive degradation of the matrix starting from 6 days of incubation at 37℃ in the presence of cells. At 17 days, when the matrix integrity is seriously degraded, the presence of the fluorescent protein in cells is no longer seen.

The flow cytometry results depicting the level of fluorescent protein expression induced by polyplexes C60-PEI/pEYFP free or embedded in matrix over time are shown in Figure 45. At defined time points, cells were harvested from culture plates and investigated using flow cytometry. It can be observed a high percentage of cells expressing YFP protein (approx. 45%) at 3 days of incubation of the cells with matrix containing C60-PEI/pEYFP polyplexes. By comparison, the incubation of cells with free C60-PEI/pEYFP polyplexes induces the expression of fluorescent protein in more than 65% cells at 3 days and about 20 % cells express fluorescent protein after 6 days.

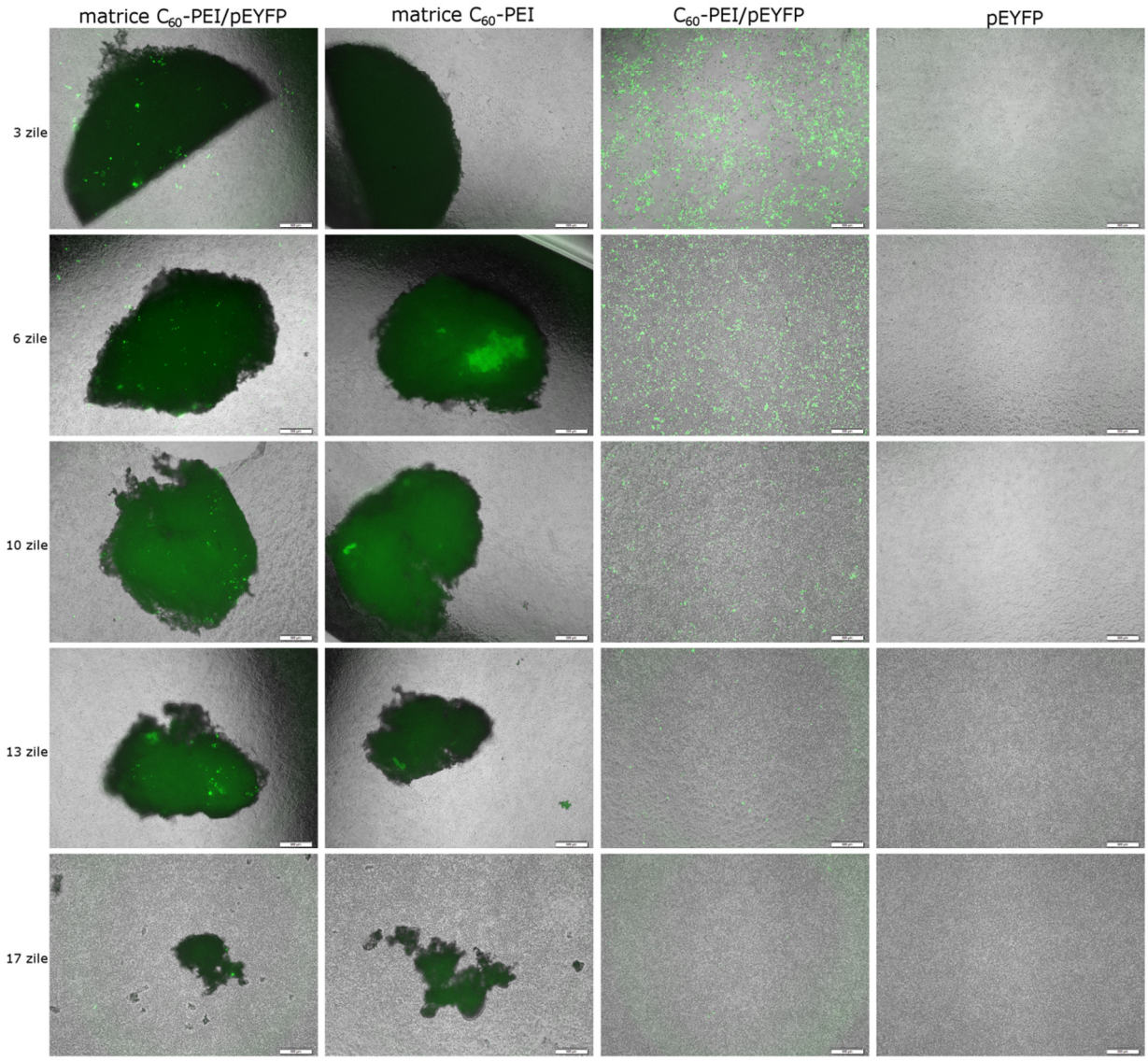

Figure 44. *Fluorescent protein expression in HEK 293T cells incubated in the presence of matrix containing polyplexes formed between C60-PEI included in the matrix walls and pEYFP at a ratio N/P =30. As a control, are shown images obtained when using matrix in the absence of pEYFP and images obtained when transfection was performed with free polyplexes C60-PEI/ pEYFP (N/P = 30) or free pEYFP plasmid. The images represent the overlap between fluorescence and phase contrast images. Bar: 500 µm.*

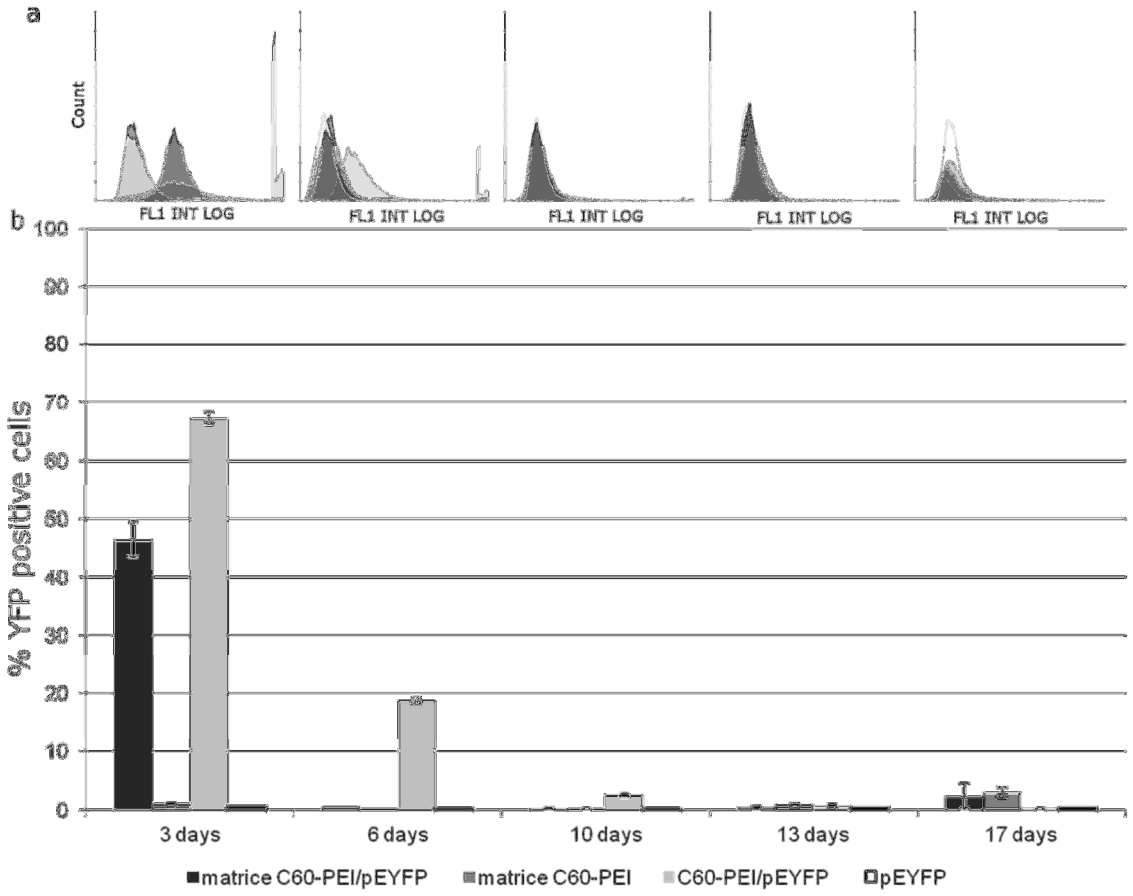

Figure 45. *The expression of fluorescent protein YFP in HEK 293T cells incubated with polyplexes formed between C60-PEI immobilized matrix and pEYFP (matrix C60-PEI/pEYFP), matrix without plasmid (matrix C60-PEI), free polyplexes (C60-PEI/pEYFP) and free pDNA (pEYFP), analyzed over time using flow cytometry. Histograms present cell count versus fluorescence measured in FL1 channel (a) and statistical representation of % of YFP protein positive cells (b).*

The effect of matrix degradation products on the viability of HEK 293T cells

It has been followed the viability of HEK 293T cells at 48 hours of incubation in the presence of degradation products after incubation of the matrix containing the vector C60-PEI immobilized in the walls, in the absence or presence of plasmid pEYFP (to obtain a ratio N/P = 30 with C60-PEI) for 24, 48 and 72 hours at 37℃ in DMEM culture medium supplemented with 10% fetal bovine serum. Results of a representative experiment performed in triplicates for cells incubated with matrix degradation products are shown in Figure 46. It can be seen a decrease in cellular viability by about 20% for matrix containing C60-PEI in the walls in the presence or absence of pEYFP at N/P = 30. Incubation with solutions of plasmid exposed to 37℃ for various times had no effect

on cell viability, whereas the incubation with solutions containing free C60-PEI/pEYFP polyplexes (N/P=30) causes a decrease in viability with about 30-40%.

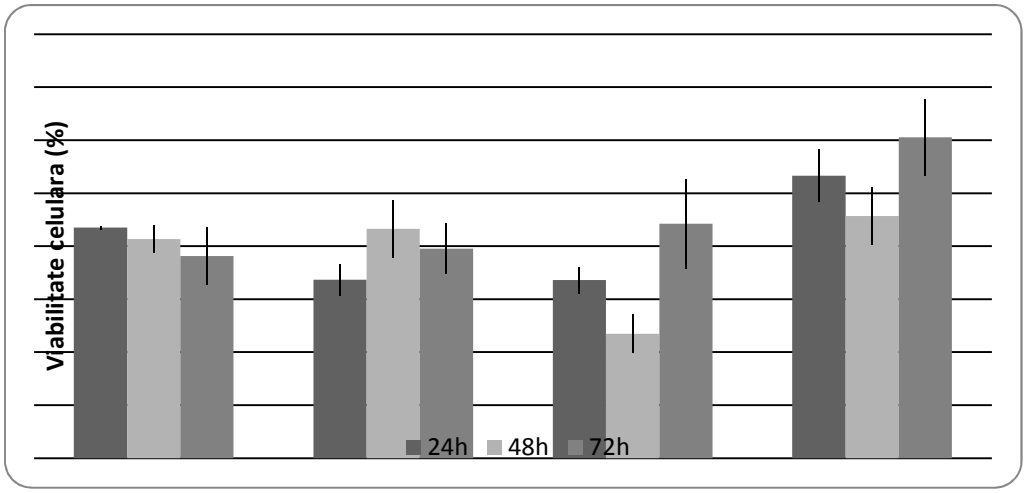

***Figure 46**. Cytotoxicity of degradation products resulted after incubation at 37℃ in mediu with serum for various times of the matrix containing the vector C60-PEI immobilized in the walls, in the absence or presence of plasmid pEYFP or free polyplexes C60-PEI/pEYFP and free plasmid pEYFP on HEK 293T cells. The results are expressed as a percentage of control cells incubated in culture medium in the absence of degradation products which was considered 100% viability.*

In conclusion in the case of the matrix constructed with C60-PEI immobilized in the walls:

(1) the polyplexes obtained with a plasmid encoding a variant of green fluorescent protein (pEYFP) at an N/P=30 determine the expression of protein encoded by the plasmid in about 40% of cells incubated in the presence of matrix/polyplexes for 3 days. Cells expressing the fluorescent protein can be observed for periods of time up to 13 days of culturing in the presence of matrix C60-PEI/pEYFP. The degradation of matrix occurs gradually, and at 17 days of incubation an advanced degradation is observed. No obvious cytotoxicity of matrix/polyplexes was noticed on HEK 293T cells;

(2) The degradation products of matrices containing C60-PEI resulting from incubation of matrices in culture medium with serum for 24, 48, 72 hours did not have a drastic effect on cell viability, causing a decrease in cell viability by approximately 20% after 48 hour of incubation of the HEK 293T cells in the presence of matrix degradation products.

Synoptic:

- published papers: **15**;
- accepted papers: **4** (till 27.11.2015);
- conference papers: **3**;
- submitted papers: **8**;
- conference communications: **22**;
- poster presentations: **15**.
- scientific stays: ;
- PhD thesis with acknowledges for the project: Andrei, alina, etc.

Published papers

Accepted papers

Submitted papers

Conference communications

Poster presentations

Scientific stays: ;

- PhD thesis with acknowledges for the project: Andrei, alina, etc.

Patents;

References

(1) Kitano, S.; Kataoka, K.; Koyama, Y.; Okano, T.; Sakurai, Y. Glucose-responsive Complex Formation between Poly (Vinyl Alcohol) and Poly (N-vinyl-2-pyrrolidone) with Pendent Phenylboronic Acid Moieties. *Makromol. Chem. Rapid Commun.* **1991**, *12*, 227–233.

(2) Kitano, S.; Koyama, Y.; Kataoka, K.; Okano, T.; Sakurai, Y. A Novel Drug Delivery System Utilizing a Glucose Responsive Polymer Complex between Poly (Vinyl Alcohol) and Poly (N-Vinyl-2-Pyrrolidone) with a Phenylboronic Acid Moiety. *J. Controlled Release* **1992**, *19*, 161–170.

(3) Keita, G.; Ricard, A.; Audebert, R.; Pezron, E.; Leibler, L. The Poly (Vinyl Alcohol)-Borate System: Influence of Polyelectrolyte Effects on Phase Diagrams. *Polymer* **1995**, *36*, 49–54.
(4) Peters, G. M.; Skala, L. P.; Plank, T. N.; Hyman, B. J.; Manjunatha Reddy, G.; Marsh, A.; Brown, S. P.; Davis, J. T. A G4· K+ Hydrogel Stabilized by an Anion. *J. Am. Chem. Soc.* **2014**, *136*, 12596–12599.
(5) Peters, G. M.; Skala, L. P.; Plank, T. N.; Oh, H.; Manjunatha Reddy, G.; Marsh, A.; Brown, S. P.; Raghavan, S. R.; Davis, J. T. G4-Quartet· M+ Borate Hydrogels. *J. Am. Chem. Soc.* **2015**, *137*, 5819–5827.
(6) Yu, Y.; Nakamura, D.; DeBoyace, K.; Neisius, A. W.; McGown, L. B. Tunable Thermoassociation of Binary Guanosine Gels. *J. Phys. Chem. B* **2008**, *112*, 1130–1134.
(7) Buerkle, L. E.; Rowan, S. J. Supramolecular Gels Formed from Multi-Component Low Molecular Weight Species. *Chem. Soc. Rev.* **2012**, *41*, 6089–6102.
(8) Wenz, G.; Han, B.-H.; Müller, A. Cyclodextrin Rotaxanes and Polyrotaxanes. *Chem. Rev.* **2006**, *106*, 782–817.
(9) Harada, A.; Takashima, Y.; Yamaguchi, H. Cyclodextrin-Based Supramolecular Polymers. *Chem. Soc. Rev.* **2009**, *38*, 875–882.
(10) Nepogodiev, S. A.; Stoddart, J. F. Cyclodextrin-Based Catenanes and Rotaxanes. *Chem. Rev.* **1998**, *98*, 1959–1976.
(11) Marangoci, N.; Maier, S. S.; Ardeleanu, R.; Arvinte, A.; Fifere, A.; Petrovici, A. R.; Nicolescu, A.; Nastasa, V.; Mares, M.; Pasca, S. A. Low Toxicity β-Cyclodextrin-Caged 4, 4′-Bipyridinium-Bis (Siloxane): Synthesis and Evaluation. *Chem. Res. Toxicol.* **2014**, *27*, 546–557.
(12) Fifere, A.; Marangoci, N.; Maier, S.; Coroaba, A.; Maftei, D.; Pinteala, M. Theoretical Study on β-Cyclodextrin Inclusion Complexes with Propiconazole and Protonated Propiconazole. *Beilstein J. Org. Chem.* **2012**, *8*, 2191–2201.
(13) Silion, M.; Dascalu, A.; Simionescu, B. C.; Pinteala, M.; Ungurenasu, C. Synthesis and anti-HIV Activity of β-cyclodextrin-C6-sulfate/3-azido-3′-deoxythymidine Inclusion Complex. *J. Polym. Sci. Part Polym. Chem.* **2011**, *49*, 1730–1733.
(14) Hazel, P.; Huppert, J.; Balasubramanian, S.; Neidle, S. Loop-Length-Dependent Folding of G-Quadruplexes. *J. Am. Chem. Soc.* **2004**, *126*, 16405–16415.
(15) Plank, T. N.; Davis, J. T. AG 4· K+ Hydrogel That Self-Destructs. *Chem. Commun.* **2016**, *52*, 5037–5040.
(16) Elouahabi, A.; Ruysschaert, J.-M. Formation and Intracellular Trafficking of Lipoplexes and Polyplexes. *Mol. Ther.* **2005**, *11*, 336–347.
(17) Wang, T.; Upponi, J. R.; Torchilin, V. P. Design of Multifunctional Non-Viral Gene Vectors to Overcome Physiological Barriers: Dilemmas and Strategies. *Int. J. Pharm.* **2012**, *427*, 3–20.

(18) Lungwitz, U.; Breunig, M.; Blunk, T.; Göpferich, A. Polyethylenimine-Based Non-Viral Gene Delivery Systems. *Eur. J. Pharm. Biopharm.* **2005**, *60*, 247–266.
(19) Allain, V.; Bourgaux, C.; Couvreur, P. Self-Assembled Nucleolipids: From Supramolecular Structure to Soft Nucleic Acid and Drug Delivery Devices. *Nucleic Acids Res.* **2012**, *40*, 1891–1903.
(20) Bui, D. T.; Nicolas, J.; Maksimenko, A.; Desmaële, D.; Couvreur, P. Multifunctional Squalene-Based Prodrug Nanoparticles for Targeted Cancer Therapy. *Chem. Commun.* **2014**, *50*, 5336–5338.
(21) Clima, L.; Peptanariu, D.; Pinteala, M.; Salic, A.; Barboiu, M. DyNAvectors: Dynamic Constitutional Vectors for Adaptive DNA Transfection. *Chem. Commun.* **2015**, *51*, 17529–17531.
(22) Ceruti, M.; Balliano, G.; Viola, F.; Cattel, L.; Gerst, N.; Schuber, F. Synthesis and Biological Activity of Azasqualenes, Bis-Azasqualenes and Derivatives. *Eur. J. Med. Chem.* **1987**, *22*, 199–208.
(23) Xu, T.; Liu, W.; Wang, S.; Shao, Z. Elucidating the Role of Free Polycationic Chains in Polycation Gene Carriers by Free Chains of Polyethylenimine or N, N, N-Trimethyl Chitosan plus a Certain Polyplex. *Int. J. Nanomedicine* **2014**, *9*, 3231.
(24) Marin, L.; Ailincai, D.; Calin, M.; Stan, D.; Constantinescu, C. A.; Ursu, L.; Doroftei, F.; Pinteala, M.; Simionescu, B. C.; Barboiu, M. Dynameric Frameworks for DNA Transfection. *ACS Biomater. Sci. Eng.* **2015**, *2*, 104–111.
(25) Ailincai, D.; Marin, L.; Shova, S.; Tuchilus, C. Benzoate Liquid Crystals with Direct Isotropic–smectic Transition and Antipathogenic Activity. *Comptes Rendus Chim.* **2016**, *19*, 556–565.
(26) Uritu, C. M.; Calin, M.; Maier, S. S.; Cojocaru, C.; Nicolescu, A.; Peptanariu, D.; Constantinescu, C. A.; Stan, D.; Barboiu, M.; Pinteala, M. Flexible Cyclic Siloxane Core Enhances the Transfection Efficiency of Polyethylenimine-Based Non-Viral Gene Vectors. *J. Mater. Chem. B* **2015**, *3*, 8250–8267.
(27) Uritu, C. M.; Varganici, C. D.; Ursu, L.; Coroaba, A.; Nicolescu, A.; Dascalu, A. I.; Peptanariu, D.; Stan, D.; Constantinescu, C. A.; Simion, V. Hybrid Fullerene Conjugates as Vectors for DNA Cell-Delivery. *J. Mater. Chem. B* **2015**, *3*, 2433–2446.
(28) Puri, J.; Singh, R.; Chahal, V. K. Silatranes: A Review on Their Synthesis, Structure, Reactivity and Applications. *Chem. Soc. Rev.* **2011**, *40*, 1791–1840.
(29) Gil, E. S.; Wu, L.; Xu, L.; Lowe, T. L. β-Cyclodextrin-Poly (β-Amino Ester) Nanoparticles for Sustained Drug Delivery across the Blood–brain Barrier. *Biomacromolecules* **2012**, *13*, 3533–3541.
(30) Ardeleanu, R.; Calin, M.; Maier, S. S.; Dascalu, A. I.; Cojocaru, C.; Uritu, C. M.; Nicolescu, A.; Silion, M.; Peptanariu, D.; Pinteala, M. Transfection-Capable PEGylated-Cyclodextrin-Containing Polycationic Nanovectors. A New Synthesis Pathway. *Beilstein J. Org. Chem.* **2016**, *sent for publication*.

(31) Nwodo, U. U.; Green, E.; Okoh, A. I. Bacterial Exopolysaccharides: Functionality and Prospects. *Int. J. Mol. Sci.* **2012**, *13*, 14002–14015.
(32) Wang, Y.; Li, C.; Liu, P.; Ahmed, Z.; Xiao, P.; Bai, X. Physical Characterization of Exopolysaccharide Produced by Lactobacillus Plantarum KF5 Isolated from Tibet Kefir. *Carbohydr. Polym.* **2010**, *82*, 895–903.
(33) Li, W.; Mutuvulla, M.; Chen, X.; Jiang, M.; Dong, M. Isolation and Identification of High Viscosity-Producing Lactic Acid Bacteria from a Traditional Fermented Milk in Xinjiang and Its Role in Fermentation Process. *Eur. Food Res. Technol.* **2012**, *235*, 497–505.
(34) Tayuan, C.; Tannock, G. W.; Rodtong, S. Growth and Exopolysaccharide Production by Weissella Sp. from Low-Cost Substitutes for Sucrose. *Afr. J. Microbiol. Res.* **2011**, *5*, 3693–3710.
(35) Palomba, S.; Cavella, S.; Torrieri, E.; Piccolo, A.; Mazzei, P.; Blaiotta, G.; Ventorino, V.; Pepe, O. Wheat Sourdough from Leuconostoc Lactis and Lactobacillus Curvatus Exopolysaccharide-Producing Starter Culture: Polyphasic Screening, Homopolysaccharide Composition and Viscoelastic Behavior. *Appl. Environ. Microbiol.* **2012**, AEM-07302.
(36) Xiao, Q.; Tong, Q.; Lim, L.-T. Drying Process of Pullulan Edible Films Forming Solutions Studied by ATR-FTIR with Two-Dimensional Correlation Spectroscopy. *Food Chem.* **2014**, *150*, 267–273.
(37) Ahmed, Z.; Wang, Y.; Anjum, N.; Ahmad, H.; Ahmad, A.; Raza, M. Characterization of New Exopolysaccharides Produced by Coculturing of L. Kefiranofaciens with Yoghurt Strains. *Int. J. Biol. Macromol.* **2013**, *59*, 377–383.
(38) Samal, P. K.; Dangi, J. S. Isolation, Preliminary Characterization and Hepatoprotective Activity of Polysaccharides from Tamarindus Indica L. *Carbohydr. Polym.* **2014**, *102*, 1–7.
(39) Chen, Y.; Mao, W.; Gao, Y.; Teng, X.; Zhu, W.; Chen, Y.; Zhao, C.; Li, N.; Wang, C.; Yan, M. Structural Elucidation of an Extracellular Polysaccharide Produced by the Marine Fungus Aspergillus Versicolor. *Carbohydr. Polym.* **2013**, *93*, 478–483.
(40) van Hijum, S. A.; Kralj, S.; Ozimek, L. K.; Dijkhuizen, L.; van Geel-Schutten, I. G. Structure-Function Relationships of Glucansucrase and Fructansucrase Enzymes from Lactic Acid Bacteria. *Microbiol. Mol. Biol. Rev.* **2006**, *70*, 157–176.
(41) Maia, J.; Carvalho, R. A.; Coelho, J. F.; Simões, P. N.; Gil, M. H. Insight on the Periodate Oxidation of Dextran and Its Structural Vicissitudes. *Polymer* **2011**, *52*, 258–265.
(42) Stanciu, M. C.; Nichifor, M. New Biocompatible Amphiphilic Diblock Copolymer Based on Dextran. *Eur. Polym. J.* **2015**, *71*, 352–363.
(43) Bucatariu, S.; Constantin, M.; Ascenzi, P.; Fundueanu, G. Poly (Lactide-Co-Glycolide)/Cyclodextrin (Polyethyleneimine) Microspheres for Controlled Delivery of Dexamethasone. *React. Funct. Polym.* **2016**, *107*, 46–53.

(44) Constantin, M.; Bucatariu, S.; Stoica, I.; Fundueanu, G. Smart Nanoparticles Based on Pullulan-G-poly(N-Isopropylacrylamide) for Controlled Delivery of Indomethacin. *Int. J. Biol. Macromol.* **2016**.
(45) Rosca, I.; Minea, B.; Peptanariu, D.; Marangoci, N.; Fifere, A.; Mares, M. Inclusion Complex of Propiconazole Nitrate with Substituted β-Cyclodextrin S II: In Vitro Assessment of Antifungal Properties. *J Mater. Sci Eng* **2016**, *5*, 71.
(46) Marangoci, N. L.; Minea, B.; Nicolescu, A.; Neamtu, A.; Varganici, C. D.; Rosca, I. Inclusion Complexes of Propiconazole Nitrate with Substituted β-Cyclodextrins: Synthesis, Characterization and in Silico Assessment. *J Mater. Sci Eng* **2016**, *5*, 72.
(47) Minea, B.; Marangoci, N.; Peptanariu, D.; Rosca, I.; Nastasa, V.; Corciova, A.; Varganici, C.; Nicolescu, A.; Fifere, A.; Neamtu, A. Inclusion Complexes of Propiconazole Nitrate with Substituted β-Cyclodextrins: The Synthesis and in Silico and in Vitro Assessment of Their Antifungal Properties. *New J. Chem.* **2016**, *40*, 1765–1776.
(48) Ali, S. M.; Asmat, F.; Koketsu, M. 1H NMR Spectroscopic Investigation of β-Cyclodextrin Inclusion Compounds with Parecoxib. *J. Incl. Phenom. Macrocycl. Chem.* **2007**, *59*, 191–196.
(49) Arendrup, M. C.; Cuenca-Estrella, M.; Lass-Flörl, C.; Hope, W. EUCAST Technical Note on the EUCAST Definitive Document EDef 7.2: Method for the Determination of Broth Dilution Minimum Inhibitory Concentrations of Antifungal Agents for Yeasts EDef 7.2 (EUCAST-AFST). *Clin. Microbiol. Infect.* **2012**, *18*, E246–E247.
(50) Andrews, J. M. Determination of Minimum Inhibitory Concentrations. *J. Antimicrob. Chemother.* **2001**, *48*, 5–16.
(51) CellTiter 96(R) AQueous One Solution Cell Proliferation Assay Technical Bulletin TB245 - celltiter-96-aqueous-one-solution-cell-proliferation-assay-system-protocol.pdf https://www.promega.com/-/media/files/resources/protocols/technical-bulletins/0/celltiter-96-aqueous-one-solution-cell-proliferation-assay-system-protocol.pdf (accessed Sep 16, 2016).
(52) Bravo-Suárez, J. J.; Páez-Mozo, E. A.; Oyama, S. T. Microtextural Properties of Layered Double Hydroxides: A Theoretical and Structural Model. *Microporous Mesoporous Mater.* **2004**, *67*, 1–17.
(53) Rives, V.; del Arco, M.; Martín, C. Layered Double Hydroxides as Drug Carriers and for Controlled Release of Non-Steroidal Antiinflammatory Drugs (NSAIDs): A Review. *J. Controlled Release* **2013**, *169*, 28–39.
(54) San Román, M.; Holgado, M.; Salinas, B.; Rives, V. Characterisation of Diclofenac, Ketoprofen or Chloramphenicol Succinate Encapsulated in Layered Double Hydroxides with the Hydrotalcite-Type Structure. *Appl. Clay Sci.* **2012**, *55*, 158–163.

(55) Del Arco, M.; Fernández, A.; Martín, C.; Rives, V. Release Studies of Different NSAIDs Encapsulated in Mg, Al, Fe-Hydrotalcites. *Appl. Clay Sci.* **2009**, *42*, 538–544.
(56) Yang, J.-H.; Han, Y.-S.; Park, M.; Park, T.; Hwang, S.-J.; Choy, J.-H. New Inorganic-Based Drug Delivery System of Indole-3-Acetic Acid-Layered Metal Hydroxide Nanohybrids with Controlled Release Rate. *Chem. Mater.* **2007**, *19*, 2679–2685.
(57) Gao, Y.; Yuan, J.; Liu, H.; Yang, Y.; Hou, Y.; Li, S. Tramadol Loading, Release and Iontophoretic Characteristics of Ion-Exchange Fiber. *Int. J. Pharm.* **2014**, *465*, 102–111.
(58) Alexandrica, M. C.; Silion, M.; Timpu, D.; Popa, M. I. A Study on the Intercalation Process of Tramadol Hydrochloride in ZnAl - Nitrate Layered Double Hydroxides. *Rev. Roum. Chim.* **2016**, *61*, accepted.
(59) Bonadio, J.; Smiley, E.; Patil, P.; Goldstein, S. Localized, Direct Plasmid Gene Delivery in Vivo: Prolonged Therapy Results in Reproducible Tissue Regeneration. *Nat. Med.* **1999**, *5*, 753–759.
(60) Fang, J.; Zhu, Y.-Y.; Smiley, E.; Bonadio, J.; Rouleau, J. P.; Goldstein, S. A.; McCauley, L. K.; Davidson, B. L.; Roessler, B. J. Stimulation of New Bone Formation by Direct Transfer of Osteogenic Plasmid Genes. *Proc. Natl. Acad. Sci.* **1996**, *93*, 5753–5758.
(61) Keeney, M.; van den Beucken, J. J.; van der Kraan, P. M.; Jansen, J. A.; Pandit, A. The Ability of a Collagen/Calcium Phosphate Scaffold to Act as Its Own Vector for Gene Delivery and to Promote Bone Formation via Transfection with VEGF 165. *Biomaterials* **2010**, *31*, 2893–2902.
(62) Scherer, F.; Schillinger, U.; Putz, U.; Stemberger, A.; Plank, C. Nonviral Vector Loaded Collagen Sponges for Sustained Gene Delivery in Vitro and in Vivo. *J. Gene Med.* **2002**, *4*, 634–643.
(63) Cohen-Sacks, H.; Elazar, V.; Gao, J.; Golomb, A.; Adwan, H.; Korchov, N.; Levy, R. J.; Berger, M. R.; Golomb, G. Delivery and Expression of pDNA Embedded in Collagen Matrices. *J. Controlled Release* **2004**, *95*, 309–320.
(64) Cao, X.; Deng, W.; Wei, Y.; Yang, Y.; Su, W.; Wei, Y.; Xu, X.; Yu, J. Incorporating pTGF-beta1/Calcium Phosphate Nanoparticles with Fibronectin into 3-Dimensional Collagen/Chitosan Scaffolds: Efficient, Sustained Gene Delivery to Stem Cells for Chondrogenic Differentiation. *Eur Cell Mater* **2012**, *23*.
(65) Raftery, R. M.; Walsh, D. P.; Castaño, I. M.; Heise, A.; Duffy, G. P.; Cryan, S.; O'Brien, F. J. Delivering Nucleic-Acid Based Nanomedicines on Biomaterial Scaffolds for Orthopedic Tissue Repair: Challenges, Progress and Future Perspectives. *Adv. Mater.* **2016**.